

University of Dundee

Measuring root system traits of wheat in 2D images to parameterize 3D root architecture models

Landl, Magdalena; Schnepf, Andrea ; Vanderborght, Jan; Bengough, Anthony; Bauke, Sara L.; Lobet, Guillaume

Published in:
Plant and Soil

DOI:
[10.1007/s11104-018-3595-8](https://doi.org/10.1007/s11104-018-3595-8)

Publication date:
2018

Document Version
Peer reviewed version

[Link to publication in Discovery Research Portal](#)

Citation for published version (APA):

Landl, M., Schnepf, A., Vanderborght, J., Bengough, A., Bauke, S. L., Lobet, G., Bol, R., & Vereecken, H. (2018). Measuring root system traits of wheat in 2D images to parameterize 3D root architecture models. *Plant and Soil*, 425(1-2), 457-477. <https://doi.org/10.1007/s11104-018-3595-8>

General rights

Copyright and moral rights for the publications made accessible in Discovery Research Portal are retained by the authors and/or other copyright owners and it is a condition of accessing publications that users recognise and abide by the legal requirements associated with these rights.

- Users may download and print one copy of any publication from Discovery Research Portal for the purpose of private study or research.
- You may not further distribute the material or use it for any profit-making activity or commercial gain.
- You may freely distribute the URL identifying the publication in the public portal.

Take down policy

If you believe that this document breaches copyright please contact us providing details, and we will remove access to the work immediately and investigate your claim.

“This is a post-peer-review, pre-copyedit version of an article published in Plant and Soil. The final authenticated version is available online at: <https://doi.org/10.1007/s11104-018-3595-8>”.

Plant and Soil

Measuring root system traits of wheat in 2D images to parameterize 3D root architecture models

--Manuscript Draft--

Manuscript Number:	PLSO-D-17-01451R1	
Full Title:	Measuring root system traits of wheat in 2D images to parameterize 3D root architecture models	
Article Type:	Manuscript	
Keywords:	axial root trajectories; branching angle; foraging performance; inter-branch distance; model parameterization; root system architecture	
Corresponding Author:	Magdalena Landl, M.Sc. Forschungszentrum Julich Jülich, Nordrhein-Westfalen GERMANY	
Corresponding Author Secondary Information:		
Corresponding Author's Institution:	Forschungszentrum Julich	
Corresponding Author's Secondary Institution:		
First Author:	Magdalena Landl, M.Sc.	
First Author Secondary Information:		
Order of Authors:	Magdalena Landl, M.Sc.	
	Andrea Schnepf, Prof.	
	Jan Vanderborght, Prof.	
	Glyn Anthony Bengough, Ph.D	
	Sara Louise Bauke, M.Sc.	
	Guillaume Lobet, Prof.	
	Roland Bol, Ph.D	
	Harry Vereecken, Prof.	
Order of Authors Secondary Information:		
Funding Information:	Deutsche Forschungsgemeinschaft (PAK888)	Ms. Magdalena Landl
Abstract:	<p>Background and aims The main difficulty in the use of 3D root architecture models is correct parameterization. We evaluated distributions of the root traits inter-branch distance, branching angle and axial root trajectories from contrasting experimental systems to improve model parameterization.</p> <p>Methods We analyzed 2D root images of different wheat varieties (Triticum Aestivum) from three different sources using automatic root tracking. Model input parameters and common parameter patterns were identified from extracted root system coordinates. Simulation studies were used to (1) link observed axial root trajectories with model input parameters (2) evaluate errors due to the 2D (versus 3D) nature of image sources and (3) investigate the effect of model parameter distributions on root foraging performance.</p> <p>Results Distributions of inter-branch distances were approximated with lognormal functions. Branching angles showed mean values <90°. Gravitropism and tortuosity parameters were quantified in relation to downwards reorientation and segment angles of root axes. Root system projection in 2D increased the variance of branching angles. Root foraging performance was very sensitive to parameter distribution and variance.</p> <p>Conclusions 2D image analysis can systematically and efficiently analyze root system architectures and parameterize 3D root architecture models. Effects of root system</p>	

1 **Measuring root system traits of wheat in** 2 **2D images to parameterize 3D root** 3 **architecture models**

4 Magdalena Landl (1)*, Andrea Schnepf (1), Jan Vanderborght (1), A. Glyn
5 Bengough (2, 3), Sara L. Bauke (4), Guillaume Lobet (1), Roland Bol (1) and
6 Harry Vereecken (1)

7

8 **Affiliation**

9 (1) Forschungszentrum Juelich GmbH, Agrosphere (IBG-3), D- 52428 Juelich,
10 Germany

11 (2) The James Hutton Institute, Invergowrie, Dundee, DD2 5DA, UK

12 (3) School of Science and Engineering, University of Dundee, Dundee DD1
13 4HN, UK

14 (4) Institute of Crop Science and Resource Conservation (INRES) – Soil
15 Science and Soil Ecology, University of Bonn, Nussallee 13, 53115 Bonn,
16 Germany

17 *Corresponding author: Email: m.landl@fz-juelich.de

18

19 *Corresponding author:

20 Magdalena Landl

21 Forschungszentrum Juelich GmbH, Agrosphere (IBG-3)

22 D- 52428 Juelich, Germany

23 Tel.: +49 2461 61 8835

24 Fax: +49 2461 61 2518

25 m.landl@fz-juelich.de

26

27 Number of text pages: 32

28 Number of tables: 6

29 Number of figures: 16

30

31 **Keywords**

32 axial root trajectories, branching angle, foraging performance, inter-branch
33 distance, model parameterization, root system architecture

34 **Abstract**

35 *Background and aims* The main difficulty in the use of 3D root architecture
36 models is correct parameterization. We evaluated distributions of the root traits
37 inter-branch distance, branching angle and axial root trajectories from
38 contrasting experimental systems to improve model parameterization.

39 *Methods* We analyzed 2D root images of different wheat varieties (*Triticum*
40 *Aestivum*) from three different sources using automatic root tracking. Model
41 input parameters and common parameter patterns were identified from extracted
42 root system coordinates. Simulation studies were used to (1) link observed axial
43 root trajectories with model input parameters (2) evaluate errors due to the 2D
44 (versus 3D) nature of image sources and (3) investigate the effect of model
45 parameter distributions on root foraging performance.

46 *Results* Distributions of inter-branch distances were approximated with
47 lognormal functions. Branching angles showed mean values $<90^\circ$. Gravitropism
48 and tortuosity parameters were quantified in relation to downwards reorientation
49 and segment angles of root axes. Root system projection in 2D increased the
50 variance of branching angles. Root foraging performance was very sensitive to
51 parameter distribution and variance.

52 *Conclusions* 2D image analysis can systematically and efficiently analyze root
53 system architectures and parameterize 3D root architecture models. Effects of
54 root system projection (2D from 3D) and deflection (at rhizotron face) on size
55 and distribution of particular parameters are potentially significant.

56 **Abbreviations**

57 β , root segment angle to the horizontal

58 $\Delta\beta$, reorientation angle of an individual root segment

59 D_e , diffusion coefficient of a solute in soil

60 ibd, inter-branch distance

61 IRC, inter-root competition

62 μ , mean value

63 σ , standard deviation of the random deflection angle (tortuosity)

64 sg, sensitivity to gravitropism

65 std, standard deviation

66 θ , branching angle in the vertical plane

67 **Introduction**

68 The efficiency of a plant root system to acquire below-ground resources
69 predominantly depends on its root system architecture (Lynch 2007; Rich and
70 Watt 2013; Smith and De Smet 2012). The complex process of root system
71 development and its interaction with the soil matrix is, however, hard to study
72 due to the opaque nature of the soil which makes direct measurements difficult.
73 The use of three - dimensional root architecture models can thereby provide an
74 opportunity to systematically investigate the influence of different

75 environmental conditions and a wide range of crop management regimes on the
76 formation and functionality of root systems, to interpret experimental data and to
77 test hypotheses on root – soil interaction processes at different scales (Dunbabin
78 et al. 2013; Roose and Schnepf 2008). In experimental field studies, such large
79 scale testing approaches are impossible to realize. An important prerequisite for
80 this simulation based investigation is that properties and behavior of the root
81 system that define its functioning in soils under different conditions can be
82 inferred from experimental data.

83 Over the years, several three-dimensional root architectural models have been
84 developed: RootMap (Diggle 1988), R-SWMS (Javaux et al. 2008), RootBox
85 (Leitner et al. 2010), SimRoot (Lynch et al. 1997), RootTyp (Pagès et al. 2004),
86 SPACSYS (Wu et al. 2007). This diversity can be explained by the wide range
87 of specific model objectives such as representation of architectural
88 characteristics of different species (Diggle 1988; Pagès et al. 2004), analysis of
89 interactions between root development and water and nutrient uptake (Dunbabin
90 et al. 2002) or investigation of root growth in structured soil (Landl et al. 2017).
91 The gross representation of root systems, however, is comparable in all these
92 models and they use similar root architectural parameter sets: While the total
93 size of a root system is mainly determined by root traits regulating the branching
94 density such as inter-branch distance, the shape or distribution of a root system
95 depends essentially on branching angle and root growth trajectories of the main
96 axes (Bingham and Wu 2011). Root growth trajectories of the main axes are
97 determined by the directional orientation of newly developed root segments.
98 Due to the ability to use both space and time dimensions as well as various
99 model concepts, parameters that are used in models that generate root
100 architectures can be defined in several ways. Table 1 gives an overview of the
101 parameterization of the root traits inter-branch distance, branching angle and

102 root growth trajectories of the main axes for several individual root architecture
103 models.

104 Differences in the parameterization of root traits leads to changes in root system
105 architecture, which significantly affects the ability of roots to forage the soil and
106 thus the root nutrient uptake capacity (Fitter et al 1991; Pagès 2011). Correct
107 parameterization of 3D root architecture models is thus crucial when evaluating
108 root-soil interaction processes.

109 Root architecture parameterization techniques always represent a compromise
110 between throughputs, precision, realistic representation of field root
111 architectures and ease of data processing (Kuijken et al. 2015). While 3D
112 imaging techniques such as x-ray computed tomography (Mooney et al. 2012;
113 Tracy et al. 2012; Tracy et al. 2010) and magnetic resonance imaging
114 (Pohlmeier et al. 2013; Rascher et al. 2011) allow non – invasive studying of the
115 spatio – temporal dynamics of root growth, they still require elaborate data
116 processing and are only suitable for relatively small and young root systems
117 scanned at low throughput rate (Mairhofer et al. 2012; Nagel et al. 2012).
118 Destructive sampling allows measurement of the whole root system, however, it
119 is a time consuming and tedious work, natural root positions can hardly be kept
120 and a large loss of fine roots must be accepted (Judd et al. 2015; Pagès and
121 Pellerin 1994; Pellerin and Pagès 1994). In that sense, root parameterization via
122 2D image analysis represents a good alternative by allowing for various methods
123 of image acquisition, high throughput and – due to recent developments of
124 automated root tracking software – relatively simple processing (Delory et al.
125 2016; Leitner et al. 2014).

126 Various methods for the acquisition of 2D root images have been developed
127 over the years: The first 2D representations of root system architecture were
128 hand drawings (Kutschera 1960; Lichtenegger et al. 2009; Weaver et al. 1922;

129 Weaver et al. 1924). The field grown root systems were thereby gradually
130 excavated and simultaneously traced on sketching paper (Kutschera 1960). A
131 recently-revived method to non-invasively image the development of root
132 system architecture in 2D is that of imaging roots grown in rhizotrons, and
133 specifically rhizotron boxes (Kuchenbuch and Ingram 2002; Nagel et al. 2012).
134 Rhizotron boxes are soil filled containers with a transparent front plate that
135 allows observing dynamic changes in root system architecture. While rhizotrons
136 enable better control of environmental influences on root architecture
137 development, they spatially constrict the root system and allow only partial
138 visibility of roots at the transparent front plate (Nagel et al. 2012; Nagel et al.
139 2015; Wenzel et al. 2001). A simple method that produces a large number of
140 images with perfect visibility of the root system is represented by roots grown
141 on germination paper (Atkinson et al. 2017; Atkinson et al. 2015). The absence
142 of soil structure and soil mechanical impedance as well the limited root age,
143 however, cast doubt if the observed root architecture is a valid representation of
144 root systems of field grown plants (Clark et al. 2011; Hargreaves et al. 2009;
145 Nagel et al. 2012).

146 In this study, we want to recover the root traits inter-branch distance, branching
147 angle and root growth trajectories of the main axes from various 2D root images
148 of different wheat varieties (*Triticum Aestivum*). Model input parameters and
149 common parameter patterns are identified. In a series of simulation studies
150 possible parameterization errors due to the two-dimensionality of image sources
151 as well as the influence of different parameterizations on root foraging
152 performance are evaluated.

153 **Materials and Methods**

154 Image Sources

155 We used root images from three different sources: hand drawings from
156 literature, images from a rhizotron experiment and images from roots grown on
157 germination paper (Fig.1). The 11 hand drawings with image resolutions
158 between 85 and 270 ppi were selected from three different literature sources and
159 represent root systems of variable age and wheat varieties growing at diverse
160 locations (Table 2). The rhizotron images with a resolution of 300 ppi were
161 obtained from an experimental study, in which spring wheat was grown under
162 controlled laboratory conditions in rhizotrons with inner dimensions of
163 50x30x3.5 cm. The lower part of the rhizotrons was filled with compacted
164 subsoil, the upper part with loose topsoil (bulk density 1.4 g cm^{-3} and 1 g cm^{-3}
165 respectively). While the experimental setup included different topsoil treatments
166 with regard to phosphorus and water supply, we only used the images of the six
167 control replicates where both phosphorus and water supply was sufficient. The
168 rhizotron images were taken on day 41 after sowing, just before harvest. A
169 detailed description of the experimental setup is given in (Bauke et al. 2017).
170 The images of roots grown on germination paper (24x30 cm) with a resolution
171 of 442 ppi were obtained from an experimental study, where two different
172 winter wheat cultivars ('Rialto' and 'Savannah') were grown in 41 respectively
173 39 replicates over a time period of 8 days under controlled lab conditions. A
174 detailed description of the experimental setup is given in Atkinson et al. (2015).

175 Image Analysis

176 Root system images were processed using the fully automatic root tracking
177 software Root System Analyzer which is based on MATLAB (R2014b) (RSA;

178 Leitner et al. 2014). The RSA saves detailed information on the coordinates of a
179 root system in MATLAB mat-files. Analysis with the RSA requires images with
180 continuous and clearly visible root systems. The rhizotron images, where only
181 part of the total root system is visible at the transparent front plate of the
182 rhizotron, thus had to be pre-processed prior to analysis. We used the open
183 source tool GIMP 2.8 to segment the root systems manually. To keep error
184 propagation from image segmentation to parameter determination at a minimum,
185 we first only segmented those roots, which were clearly visible on the rhizotron
186 image. These root systems were later used for recovering the parameters
187 branching angle and axial trajectories. We then additionally inserted laterals, for
188 which we had to estimate the location of the connection to their parent root.
189 These extended root systems were later used for recovering the parameter inter-
190 branch distance, which depends on the visibility of all lateral roots.

191 Root Parameter Analysis

192 We parameterized the root traits inter-branch distance, branching angle and root
193 growth trajectories of the main axes from the extracted root system coordinates.
194 The inter-branch distance was measured as the distance between two successive
195 branches in centimeters. The branching angle was determined as the angle in the
196 vertical plane between a branch and its parent root in degrees, which is
197 measured at a certain distance from the point where the branch emerges. In one
198 respect, this distance should be minimized to measure the initial branching
199 angle; however, it also needs to be large enough to avoid inaccuracies in the
200 computation process. We performed a small analysis based on artificial root
201 systems with known ground truth and similar root radii, which suggested that a
202 search radius of 0.5 cm distance from the branch point is suitable for correctly
203 computing branching angles. Root growth trajectories of axial roots are
204 determined by their initial growth angle from the horizontal and its dynamic

205 changes from the root base to the root apex which is affected by numerous
206 factors such as soil compaction (Popova et al. 2016), soil temperature (Tardieu
207 and Pellerin 1990) or soil water status (Nakamoto 1994). In a simplified way,
208 the shape of a root trajectory can be described by two features: its overall
209 curvature and its small-scale waviness which is known as tortuosity (Popova et
210 al. 2016). To characterize the axial root trajectories from our data sources, we
211 divided each root into segments of 1 cm length and determined for each segment
212 its angle to the horizontal as well as its reorientation angle with respect to the
213 previous root segment in degrees. We then calculated the relationship between
214 growth angle and reorientation angle of individual root segments, which gives
215 information on the curvature of a trajectory in relation to its inclination as well
216 as on tortuosity.

217 Root parameters were quantified separately for each of the 11 root drawings.
218 Root parameters derived from the six rhizotron images obtained from replicate
219 experiments were pooled together to one group. Root parameters derived from
220 images of roots grown on germination paper were classified into two groups
221 according to cultivar ('Rialto': 39 images, 'Savannah': 41 images). Altogether,
222 we analyzed root parameters from 14 different data sources. None of the used
223 image sources allowed differentiating between seminal and shoot-born roots and
224 only one order of lateral roots was identified. We therefore only distinguish
225 between axial roots and first order laterals.

226 Simulation Studies

227 Among the different traits describing root architecture, root growth trajectories
228 of axial roots are of particular importance for the shape of a root system. Their
229 correct representation in 3D root architecture models is thus important to obtain
230 plausible simulation results. In a first simulation study, we therefore tested the

231 ability of different model approaches to reproduce our experimental findings on
232 axial root trajectories and quantified model parameters for our analyzed root
233 systems.

234 The recovery of 3D root architecture parameters from 2D images has the
235 obvious drawback of losing the third dimension. Images respectively drawings
236 of root architectures are created by projecting the 3D root systems onto 2D
237 space. Root system architectures of plants grown in rhizotrons or on germination
238 paper are affected by root deflection due to spatial growth constraints. While
239 this has no influence on the parameter inter-branch distance, both branching
240 angle and axial root growth trajectories are affected. In a second simulation
241 study, we therefore analyzed the effects of projection and deflection,
242 respectively, on the parameters branching angle and axial root growth
243 trajectories.

244 Root architecture significantly influences root foraging performance by
245 determining the volume of soil that can be explored by roots (Fitter et al. 1991;
246 Pagès 2011). In a third simulation study, we evaluated the effect of different
247 parameterizations of our focus root architecture parameters inter-branch
248 distance, branching angle and axial root growth trajectories on the foraging
249 performance of root systems.

250 Simulation study 1: Ability of 3D root architecture models to reproduce
251 experimental observations on axial root trajectories

252 In 3D root architecture models, root growth trajectories are composed of
253 individual root segments. At each root growth time step, a new segment emerges
254 whose directional orientation must be determined with regard to overall
255 curvature and tortuosity. Most root architecture models (SimRoot, RootTyp,
256 SPACSYS, R-SWMS) use a vector-based approach, where the directional

orientation of an individual root segment is calculated from a vector expressing tortuosity and a vector expressing gravitropism. 2D root images represent root systems in the xz- plane and thus provide information on root curvature and root tortuosity in vertical, but not in horizontal direction. To test the ability of the vector-based approach to reproduce observations of axial root trajectories on 2D root images, we thus converted the 3D equation to 2D space:

$$\vec{d} = \begin{pmatrix} dx_{\beta,\delta} \\ dz_{\beta,\delta} \end{pmatrix} + sg * \begin{pmatrix} 0 \\ -1 \end{pmatrix}. \quad (1)$$

The first term on the right hand side represents the growth direction vector of the preceding root segment dx_{β} with unit length 1 which is deflected by the random angle δ ; the second term expresses the gravitropism component with sg as gravitropism sensitivity factor. The random deflection angle δ is a normally distributed random angle with mean zero and unit standard deviation σ . The unknown parameters are thus the sensitivity to gravitropism sg and the standard deviation of the random deflection angle σ (cf. Clausnitzer and Hopmans (1994)). We implemented this formula in MATLAB and computed root trajectories using 7 different parameterizations of sg and 21 different parameterizations of σ (147 parameter combinations altogether, values are given in Table 3). For each parameter combination, we simulated 50 axial root trajectories with individual lengths of 50 cm (example in Fig.2).

Simulation study 2: Effects of projection and deflection on the parameters branching angle and axial root growth trajectories.

The objective of this study was to analyze the effects of projection and deflection, respectively, on the parameters branching angle and axial root growth trajectories.

281 Root system development was simulated using the MATLAB version of the 3D
282 root architecture model RootBox, which is fully described in Leitner et al.
283 (2010) and shall here only be addressed briefly. RootBox defines each root order
284 by a set of different model parameters. Basal and apical root zone determine the
285 length of the unbranched zone before the first and after the last branch,
286 respectively. Inter-branch distance defines the distance between two successive
287 branches and thereby also affects the maximum root length for a given number
288 of branches. Root growth speed is described by a negative exponential function
289 whose initial slope is determined by the initial elongation rate and whose
290 asymptote depends on the maximum root length. The emergence angle of axial
291 roots respectively the initial angle between a branch and its parent root is
292 defined by a radial angle in the horizontal plane, and an insertion respectively
293 branching angle in the vertical plane. The radial angle is generally drawn at
294 random between 0 and 2π , but can also be set to a specific angle to consider
295 non-independence of branching files. To describe axial root growth trajectories,
296 we implemented the vector-based approach used in most root architecture
297 models (SimRoot, RootTyp, SPACSYS, R-SWMS) into RootBox: In this
298 approach, newly emerged root segments are oriented according to the direction
299 of the previous root segment, sensitivity to gravitropism and random angle
300 deflection.

301 To evaluate the effect of projection, we mapped the unconstrained 3D root
302 system onto the x-z plane. To evaluate the effect of deflection, we simulated a
303 root system, which was spatially constrained by a rhizotron with dimensions of
304 20x2x30 cm (Fig.3). This geometry is implemented based on signed distance
305 functions in which the distance of a given point to the closest boundary is
306 evaluated and given a positive sign if located inside the geometry and a negative
307 sign if located outside. Random optimization ensures that the new position of a
308 growing root tip is always inside the rhizotron domain (Leitner et al. 2010).

309 Using the coordinates of these root systems, we then computed (1) branching
310 angles between laterals and their parent roots and (2) relationships between
311 angle to the horizontal and reorientation angle of individual root segments.

312 Simulation study 3: Influence of different parameterizations of inter-branch
313 distance, branching angle and axial root trajectories on foraging performance of
314 a root system

315 Root system development was simulated using the MATLAB version of the 3D
316 root architecture model RootBox with an alternative approach for the simulation
317 of axial root growth trajectories as described in simulation study 2.

318 The soil volume around a root system available for nutrient uptake, i.e. the
319 rhizosphere, was computed using the approach by Fitter et al. (1991). For this
320 procedure, a very fine 3D grid is overlaid on the root system. The center of
321 every grid cell is then scanned for its distance to the nearest root segment. If the
322 distance is smaller than a specified rhizosphere radius R_{rhiz} , the grid cell volume
323 is counted as rhizosphere volume. The rhizosphere radius R_{rhiz} is determined by
324 the effective diffusion coefficient of a solute in soil and the age of the respective
325 root segment and calculated according to Nye and Tinker (1977) as

$$326 \quad R_{rhiz} = r + 2\sqrt{D_e t}, \quad (2)$$

327 where r is the radius of the root segment (cm), D_e is the effective diffusion
328 coefficient in soil (cm^2s^{-1}) and t is the root segment age (s). To evaluate the
329 influence of different soil diffusion coefficients (D_e) on the rhizosphere volume,
330 we performed simulations with three different D_e values: 10^{-8} , 10^{-7} and 2×10^{-6}
331 $\text{cm}^2 \text{s}^{-1}$. The first two values are typical effective phosphorus diffusion
332 coefficients in soil, which account for the effect of sorption of phosphorus to soil
333 particles (Schenk and Barber 1979); the latter one is a characteristic nitrate
334 diffusion coefficient of the soil (Volder et al. 2005). While the net rhizosphere

335 volume was defined as the volumetric sum of all unique grid cells, the
 336 rhizosphere volume with overlap was specified as the volumetric sum of all -
 337 partially multiply assigned - grid cells. The overlap volume is then the
 338 difference between rhizosphere volume with overlap and net rhizosphere
 339 volume (Fig.4). Considering that both rhizosphere and overlap volume are
 340 absolute values and depend on the total size of a root system, we introduced the
 341 parameter inter-root competition (IRC) as a size-independent measure of
 342 comparison following the approach by Ge et al. (2000). IRC is calculated as

$$343 \quad IRC = \frac{V_{overlap}}{V_{rhizo}} * 100\%, \quad (3)$$

344 where $V_{overlap}$ is the overlap volume and V_{rhizo} is the net rhizosphere volume.
 345 Fig.5 shows an example of a simulated root system and its surrounding
 346 rhizosphere volume for different values of D_e .

347 Using observations from root image analysis, we identified factors that can be
 348 used to differently parameterize our three focus parameters. These factors were
 349 mean and standard deviation for both inter-branch distance and branching angle
 350 and standard deviation of the random angle deflection respectively sensitivity to
 351 gravitropism for the parameter axial root growth trajectories. For each of these
 352 factors, we defined variation intervals with lower and upper bounds. For the
 353 parameter inter-branch distance, we used probability distribution as an
 354 additional categorical factor of variation, which was set to either normal or
 355 lognormal distribution. Descriptive statistics of the lognormal distribution were
 356 calculated by transformation from the parameters of the normal distribution. The
 357 domain of the normal distribution was restricted to the positive number range;
 358 negative values were set to 10^{-6} cm. We also included a categorical factor of
 359 variation for the radial alignment of 1st order laterals around the main axis. In
 360 literature, the alignment of lateral roots around the root axis is still unclear.
 361 While Abadia-Fenoll et al. (1986) and Barlow and Adam (1988) found lateral

362 roots of onion and tomato to form in acropetal sequence around their parent axis,
363 Pellerin and Tabourel (1995) and Yu et al. (2016) observed an unpredictable
364 radial emergence pattern for lateral roots of maize and wheat. Due to these
365 inconsistencies, we specified the radial angle either as random in the interval $[0$
366 $2\pi]$ or set it to a value of 45° (sequential acropetal branching from 8 phloem
367 poles around the axis). Variation intervals for parameterization factors as well as
368 descriptions of the additional factors are given in Table 4. The remaining root
369 growth parameters were set to fixed values, which were either derived from
370 literature or directly from our analyzed root images (Table 5). We considered
371 two orders of lateral roots. The simulation time was set to 30 days and each root
372 system consisted of 7 axial roots.

373 For all possible combinations of categorical factors, we then performed 1000
374 root system realizations that corresponded with 1000 parameter sets that were
375 randomly drawn from the intervals specified in Table 4. This gave a total of
376 4000 root system realizations (i.e. $2^2 \times 1000$). For each root system, we then
377 computed inter-root competition as a measure of foraging performance for all
378 three soil diffusion coefficients (D_e) defined above. Relationships between inter-
379 root competition and our focus parameters were explored by means of
380 scatterplots. To visualize the main trends, we fitted linear regression lines.
381 Correlation analyses were then used to quantitatively evaluate the linear
382 relationship between inter-root competition and our focus parameters.

383 Statistics

384 Statistical analyses were performed with MATLAB (R2014b). To evaluate
385 differences in means with unequal variance, a Welch's t-test was used. To
386 analyze differences in variances, we performed a two-sample F-test. Linear
387 regression relationships were evaluated by means of an F-test. In the following,

388 significant results correspond to $p < 0.05$, while highly significant results
389 represent $p < 0.01$.

390 **Results**

391 Inter-branch distance

392 The relationships between inter-branch distance and distance along the root axis
393 are very scattered for all data sources with values ranging from close to 0 cm to
394 up to 3 cm. An F-test showed a significant increase in inter-branch distance from
395 the base of the branched zone down to the root apex for 11 out of 14 data sets,
396 no trend for two data sets and a decrease for one data set (Fig.6). The large
397 variability of inter-branch distances observed for the data source from rhizotron
398 images can be explained by the only partial visibility of the root system which
399 has probably obscured some lateral roots. The global distributions show for all
400 data sources a highly asymmetrical shape which can be well described with
401 lognormal distributions (Fig.7). We observed a large percentage of short inter-
402 branch distances with medians ranging between 0.1 and 0.5 cm (Fig.8). No
403 systematic pattern was apparent with regard to the different data sources.

404 Branching angle

405 The global distribution of branching angles shows a bell shape for the roots
406 grown on germination paper that can be approximated with a normal
407 distribution; for the remaining data sources, the distribution of branching angles
408 is spread more widely and shows positive skewness (Fig.9). Interestingly,
409 branching angles from all data sources show similar medians that range from
410 59.5° to 79.4° and are well below 90° (Fig.10).

411 Root growth trajectories

412 Root growth trajectories of axial roots were reconstructed for all root systems of
413 each data source from the extracted root coordinates prior to analysis (Fig.11).

414 There was a negative relationship between reorientation angle and angle of the
415 previous 1 cm long root segment for all but one data source meaning that more
416 horizontally growing roots generally reoriented stronger towards the vertical
417 than more perpendicularly growing ones (Fig.12). An F-test showed that this
418 correlation was highly significant for 3, significant for 5 and not significant for 6
419 data sources. Not significant relationships can be an indicator for abrupt changes
420 in the growth path (e.g. the rightmost trajectory in Fig 11a), high root tortuosity
421 or liminal growth angles that deviate from the vertical (Nakamoto 1994). The
422 reorientation angle $\Delta\beta$ at a segment angle of $\beta=-90^\circ$ (vertical root growth)
423 predicted by regression tended for all data sources towards zero suggesting that
424 gravitropism is the predominant influence factor in the formation of trajectory
425 curvature. While the slope of the regression line is a measure of gravitropism,
426 the standard error of the estimate determines the degree of root tortuosity. The
427 slope of the regression lines ranged between 0 and -0.2; the standard error of the
428 estimate between 7.7° and 21.8° . With regard to different data sources, we did
429 not find any systematic pattern of slope; standard errors of the estimate,
430 however, were highest for root drawings of large, mature root systems and
431 lowest for roots grown on germination paper.

432 Simulation studies

433 Simulation study 1: Ability of 3D root architecture models to reproduce
434 experimental observations on axial root trajectories

435 For each combination of parameters describing gravitropism and tortuosity, we
436 calculated the relationship between reorientation angle $\Delta\beta$ and angle of the

437 previous 1 cm long root segment β and approximated it with a linear regression
 438 line. The results are shown in Fig.13 for 20 selected parameter combinations.
 439 The standard deviation of the random deflection angle σ can be seen as a direct
 440 measure of the standard error of the estimate and thus tortuosity if the influence
 441 of gravitropism is not too strong. Large values of gravitropism force the root tip
 442 to grow towards the vertical and result in standard errors of the estimate smaller
 443 than σ . The gravitropism parameter sg is inversely proportional to the slope of
 444 the regression line. The prediction with the regression lines, which are close to
 445 0° at $\beta = -90^\circ$, reflect the minimum average reorientation of vertically oriented
 446 roots. An F-test showed that correlations between reorientation angle and angle
 447 of the previous 1 cm long root segment were highly significant for all
 448 combinations, except for the combination of the largest root tortuosity and
 449 smallest gravitropism value. The relationships between root reorientation and
 450 root angle resemble those calculated for our image-derived axial root trajectories
 451 (Fig.12). The approach is thus well suited to simulate curvature and tortuosity of
 452 wheat root trajectories.

453 To link the model parameters necessary for the simulation of root trajectories
 454 (sensitivity to gravitropism sg and root tortuosity σ) to the relationship between
 455 root reorientation and root segment angle, we calculated characteristic curves for
 456 the different parameter combinations (Fig.14). The characteristic curves are the
 457 smoothed connection lines between the properties of the regression lines
 458 (standard error of the estimate and slope) that relate segment angles and
 459 reorientation angles of axial root trajectories for each parameter combination.
 460 Figure 14 shows that slope and standard error of the regression cannot be
 461 mapped linearly to the parameters σ and sg that describe gravitropism and
 462 tortuosity. To quantify model parameters for our observed root trajectories, we
 463 inserted the regression line properties deduced from Fig.12 into the graphs and
 464 located their positions. This gave us values between 0.01 and 0.3 for the

465 sensitivity to gravitropism sg and values between 9 and 20 $^{\circ}\text{cm}^{-1}$ for the unit
466 standard deviation of the random angle σ .

467 Simulation study 2: Effects of projection and deflection on the parameters
468 branching angle and axial root growth trajectories.

469 While mean branching angles of projected and deflected root systems did not
470 differ significantly from branching angles of the unconstrained 3D root system,
471 their variance was significantly higher. This was especially true for the projected
472 root system (Fig.15-1). The similarity in mean branching angles can be
473 explained by the symmetrical alignment of lateral roots around the root axis,
474 which leads to a compensation between positive and negative angle deviations
475 due to projection or deflection. Relationships between reorientation angle and
476 angle of the previous 1 cm long root segment differed significantly between
477 projected and deflected root systems and the unconstrained 3D root system with
478 regard to slope and thus gravitropic root growth. With regard to standard
479 deviation of the estimate and thus tortuosity, only the projected, but not the
480 deflected root system showed a significantly higher value than the unconstrained
481 3D root system (Fig.15-2). Considering that absolute deviations are rather small,
482 these discrepancies in gravitropism and tortuosity are negligible in terms of
483 model parameterization.

484 Simulation study 3: Influence of different parameterizations of inter-branch
485 distance, branching angle and axial root trajectories on foraging performance of
486 a root system

487 We found clear relationships between inter-root competition and different
488 parameterizations. These relationships are illustrated for $D_e = 10^{-8} \text{ cm}^2\text{s}^{-1}$ in
489 Fig.16. In each plot, all simulation results were plotted against the specific
490 parameter. In Table 6, correlation coefficients show the significance of linear

relationships between inter-root competition and parameters. As expected, IRC decreased with increasing mean inter-branch distance. If mean inter-branch distance was low, IRC was significantly higher for lognormally than for normally distributed inter-branch distances. Regular alignment of laterals around the main axis tended to less IRC than random alignment, however, not significantly. The relationship between IRC and mean inter-branch distance was significantly weaker for the largest soil diffusion coefficient. The effect of varying standard deviation of inter-branch distance on IRC was surprising: For lognormally distributed inter-branch distances IRC increased with increasing standard deviation; for normally distributed inter-branch distances, it decreased. These relationships remained nearly constant for all soil diffusion coefficients. IRC decreased with increasing mean branching angle. This effect, however, was only significant for the lowest soil diffusion coefficient. Larger standard deviations of the branching angle led to a significant increase in IRC for the lower two soil diffusion coefficients. This effect was larger for regularly aligned laterals than for randomly aligned ones. Greater values of standard deviation of the random angle deflection led to lower IRC. This effect, however, was only significant for the largest soil diffusion coefficient. As expected, larger values of sensitivity to gravitropism led to more IRC. This effect was stronger for larger soil diffusion coefficients and also for root systems with normally distributed inter-branch distances as compared with lognormally distributed ones.

Discussion

2D image analysis is a simple and fast way to retrieve information on root system architectures for the parameterization of 3D root architecture models. The systematic analysis of root images from three different sources (root drawings, rhizotron images, images of roots grown on germination paper) allowed us to identify universally occurring parameter patterns of wheat roots.

518 Observed patterns of root architecture parameters contrast common model
519 assumptions

520 Inter-branch distance along axial roots predominantly increased with increasing
521 distance from the base of the branched zone. But in some cases, it also remained
522 constant or decreased. These results are in line with published data: While inter-
523 branch distance along the axial roots was frequently observed to increase with
524 increasing distance from the base of the branched zone (e.g. maize by Ito et al.
525 (2006), Pagès and Pellerin (1994), Postma et al. (2014) and pea by Tricot et al.
526 (1997)), other studies found constant or no identifiable pattern of inter-branch
527 distance along axial roots (e.g. wheat by Ito et al. (2006) and banana by Draye
528 (2002)). Studies have proposed that soil compaction (Pagès and Pellerin 1994),
529 oxygen gradients (Liang et al. 1996) or water availability in the vicinity of the
530 root (Bao et al. 2014) may alter branching density and thus inter-branch
531 distances. In 3D root architecture models, the phenomenon of varying inter-
532 branch distances along axial roots could be considered by a coefficient that is
533 linked to these processes. Our findings suggest that the global distribution of
534 inter-branch distances of wheat roots follows a lognormal distribution, which is
535 in line with observations by Pagès (2014) on roots of various species of the
536 Poaceae family and Le Bot et al. (2010) on the root system of a tomato plant.
537 This contrasts common assumptions of 3D root architecture models where inter-
538 branch distances are either set to a fixed value or drawn from a normal
539 distribution (see Table 1).

540 The branching angle of lateral roots relative to their parent axis is a standard
541 parameter that is included in all 3D root architecture models (Table 1) and
542 defines the initial direction of the first segment of a lateral root at the point of
543 emergence. Our findings suggest that branching angles of 1st order laterals of
544 wheat root systems are significantly smaller than 90° with a variance that

545 depends on the growth medium. This contrasts common model assumptions
546 where branching angles are frequently set to a constant value of 90° relative to
547 the parent root for reasons of simplicity (Clausnitzer and Hopmans 1994; Pagès
548 et al. 2004; Wu et al. 2005) or as a general model condition (Diggle 1988).

549 More horizontally growing roots reoriented stronger towards the vertical than
550 more vertically growing roots with reorientation angles approaching 0° as the
551 roots turn to the vertical. These findings are in line with observations by Wu et
552 al. (2015) on axial maize root trajectories. A number of axial root trajectories
553 derived from root drawings did not follow a continuous gravitropic growth path,
554 but changed their slope abruptly to the vertical after growing in relatively
555 constant direction. Similar observations were reported by Tardieu and Pellerin
556 (1990) who suggest that earthworm channels that can be used by roots as
557 preferential growth paths might be responsible for this effect. Levels of root
558 tortuosity showed a relatively clear ranking with tortuosity of root systems
559 grown in structured soil > tortuosity of roots grown in sieved soil > tortuosity of
560 roots grown on filter paper. While root age seems to have an influence, this
561 effect is probably also caused by differences in the penetration resistance of the
562 growth medium as proposed by Popova et al. (2016). A simulation study showed
563 good agreement between simulated and observed curvature and tortuosity of
564 axial wheat root trajectories. We developed characteristic curves that relate
565 model input parameters with downwards reorientation and segment angles of
566 axial trajectories. These characteristic curves can be used to calibrate the model
567 parameters gravitropism and tortuosity from 2D root trajectories, which is a step
568 forward in the realistic parameterization of 3D root architecture models.

569 Root system projection leads to overestimation of the variance of branching
570 angles

571 The use of two-dimensional root drawings or rhizotron images for the
572 parameterization of 3D root architecture models is common practice (Delory et
573 al. 2016; Doussan et al. 2006; Leitner et al. 2014; Pagès et al. 2004). To our
574 knowledge, the effects of root system projection or deflection on size and
575 distribution of 3D root architecture parameters, however, has not yet been
576 analyzed. We showed that projection greatly affects branching angles by
577 overestimating their variance. Effects of projection and deflection, respectively,
578 on tortuosity and gravitropism parameters were shown to be negligible.

579 Root foraging performance depends strongly on parameter distribution and
580 parameter variance

581 The influence of the main determinants of root architecture (e.g. mean inter-
582 branch distance, mean branching angle) on root foraging performance is well
583 documented in literature (Bingham and Wu 2011; Postma et al. 2014). The
584 influence of parameter variance and distribution, however, which describes the
585 degree to which stochasticity affects developmental processes, is much less
586 explored (Forde 2009). In most 3D root architecture models, parameter
587 stochasticity is not used or only used to a limited extent (Table 1). We could
588 demonstrate the significant impact of variance in both inter-branch distance and
589 branching angle on foraging performance of a root system. Also, the use of
590 different distributions of inter-branch distance (normal, lognormal) led to
591 significant differences in effective rhizosphere volume around a root system.
592 Interestingly, differences in radial alignment of lateral roots around the root axis,
593 i.e. random or acropetal branching, only led to minor differences in root
594 foraging performance.

595 We chose the model approach by Nye and Tinker (1977) to compute the
596 rhizosphere volume around a root system. This purely physical model assumes
597 continuous nutrient uptake by individual root segments. Gao et al. (1998) and
598 Bouma et al. (2001), however, showed that root segment age is inversely related
599 to nutrient uptake capacity and that young roots therefore take up more nutrients
600 than old roots. Inter-root competition is mainly caused by rhizosphere zone
601 overlap of neighboring laterals, which are usually of similar age. Taking into
602 account root segment age-dependent nutrient uptake rates would therefore alter
603 absolute values of root foraging performance, but not our described qualitative
604 relationships and trends.

605 This study improves the capacity of modelers to simulate realistic root systems,
606 which can be used to investigate root-soil interaction processes. Further
607 investigations could include research on parameters that were not the focus of
608 this study, but also greatly influence root foraging performance such as number
609 of axial roots, axial insertion angle and length and distribution of lateral roots.
610 More information on root architecture parameters for a range of plant species
611 would also be desirable. Increased knowledge on plastic root response to soil
612 heterogeneity and environmental changes would further improve 3D root
613 architecture modeling.

614 **Acknowledgements**

615 Funding by German Research Foundation within the Research Unit DFG PAK
616 888 is gratefully acknowledged. The James Hutton Institute receives funding
617 from the Scottish Government. We also thank Klaas Metselaar from the
618 Department of Environmental Sciences at Wageningen University, Netherlands,
619 for providing high-resolution scans of wheat root images from the Root Atlas.

620

621 Abadia-Fenoll F, Casero P, Lloret P, Vidal M 1986 Development of lateral
622 primordia in decapitated adventitious roots of *Allium cepa*. *Annals of*
623 *Botany* 58: 103-107.

624 Atkinson JA, Lobet G, Noll M, Meyer PE, Griffiths M, Wells DM 2017
625 Combining semi-automated image analysis techniques with machine
626 learning algorithms to accelerate large scale genetic studies.
627 *GigaScience* 6: 1-7.

628 Atkinson JA, Wingen LU, Griffiths M, Pound MP, Gaju O, Foulkes MJ, Le
629 Gouis J, Griffiths S, Bennett MJ, King J 2015 Phenotyping pipeline
630 reveals major seedling root growth QTL in hexaploid wheat. *Journal of*
631 *Experimental Botany* 66: 2283-2292.

632 Bao Y, Aggarwal P, Robbins NE, Sturrock CJ, Thompson MC, Tan HQ, Tham
633 C, Duan L, Rodriguez PL, Vernoux T, Mooney SJ, Bennett MJ,
634 Dinnyen JR 2014 Plant roots use a patterning mechanism to position
635 lateral root branches toward available water. *Proceedings of the*
636 *National Academy of Sciences* 111: 9319-9324.

637 Barlow P, Adam J 1988 The position and growth of lateral roots on cultured root
638 axes of tomato, *Lycopersicon esculentum* (Solanaceae). *Plant*
639 *Systematics and Evolution* 158: 141-154.

640 Bauke SL, Landl M, Koch M, Hofmann D, Nagel KA, Siebers N, Schnepf A,
641 Amelung W 2017 Macropore effects on phosphorus acquisition by
642 wheat roots – a rhizotron study. *Plant and Soil* 416: 67-82.

643 Bingham IJ, Wu L 2011 Simulation of wheat growth using the 3D root
644 architecture model SPACSYS: validation and sensitivity analysis.
645 *European Journal of Agronomy* 34: 181-189.

646 Bouma TJ, Yanai RD, Elkin AD, Hartmond U, Flores-Alva DE, Eissenstat DM
647 2001 Estimating age-dependent costs and benefits of roots with

648 contrasting life span: comparing apples and oranges. *New Phytologist*
 649 150: 685-695.

650 Clark RT, MacCurdy RB, Jung JK, Shaff JE, McCouch SR, Aneshansley DJ,
 651 Kochian LV 2011 3-dimensional root phenotyping with a novel
 652 imaging and software platform. *Plant Physiology* 156: 455-465.

653 Clausnitzer V, Hopmans J 1994 Simultaneous modeling of transient three-
 654 dimensional root growth and soil water flow. *Plant and Soil* 164: 299-
 655 314.

656 Delory BM, Baudson C, Brostaux Y, Lobet G, Du Jardin P, Pagès L, Delaplace
 657 P 2016 archiDART: an R package for the automated computation of
 658 plant root architectural traits. *Plant and Soil* 398: 351-365.

659 Diggle AJ 1988 ROOTMAP - a model in three-dimensional coordinates of the
 660 growth and structure of fibrous root systems. *Plant and Soil* 105: 169-
 661 178.

662 Doussan C, Pierret A, Garrigues E, Pagès L 2006 Water uptake by plant roots:
 663 II-Modelling of water transfer into the soil root-system with explicit
 664 account of flow within the root system - Comparison with experiments.
 665 *Plant and Soil* 283: 99-117.

666 Draye X 2002 Consequences of root growth kinetics and vascular structure on
 667 the distribution of lateral roots. *Plant, Cell & Environment* 25: 1463-
 668 1474.

669 Dunbabin V, Diggle AJ, Rengel Z, van Hugten R 2002 Modelling the
 670 interactions between water and nutrient uptake and root growth. *Plant*
 671 and *Soil* 239: 19-38.

672 Dunbabin VM, Postma JA, Schnepf A, Pagès L, Javaux M, Wu L, Leitner D,
 673 Chen YL, Rengel Z, Diggle AJ 2013 Modelling root-soil interactions
 674 using three-dimensional models of root growth, architecture and
 675 function. *Plant and Soil* 372: 93-124.

676 Fitter A, Stickland T, Harvey M, Wilson G 1991 Architectural analysis of plant
677 root systems 1. Architectural correlates of exploitation efficiency. New
678 Phytologist 118: 375-382.

679 Forde BG 2009 Is it good noise? The role of developmental instability in the
680 shaping of a root system. Journal of Experimental Botany 60: 3989-
681 4002.

682 Gao S, Pan WL, Koenig RT 1998 Integrated root system age in relation to plant
683 nutrient uptake activity. Agronomy Journal 90: 505-510.

684 Ge Z, Rubio G, Lynch JP 2000 The importance of root gravitropism for inter-
685 root competition and phosphorus acquisition efficiency: results from a
686 geometric simulation model. Plant and Soil 218: 159-171.

687 Hargreaves CE, Gregory PJ, Bengough AG 2009 Measuring root traits in barley
688 (*Hordeum vulgare* ssp. *vulgare* and ssp. *spontaneum*) seedlings using
689 gel chambers, soil sacs and X-ray microtomography. Plant and Soil
690 316: 285-297.

691 Ito K, Tanakamaru K, Morita S, Abe J, Inanaga S 2006 Lateral root
692 development, including responses to soil drying, of maize (*Zea mays*)
693 and wheat (*Triticum aestivum*) seminal roots. Physiologia Plantarum
694 127: 260-267.

695 Javaux M, Schröder T, Vanderborght J, Vereecken H 2008 Use of a Three-
696 Dimensional Detailed Modeling Approach for Predicting Root Water
697 Uptake. Vadose Zone Journal 7: 1079-1079.

698 Judd LA, Jackson BE, Fonteno WC 2015 Advancements in root growth
699 measurement technologies and observation capabilities for container-
700 grown plants. Plants 4: 369-392.

701 Kuchenbuch R, Ingram K 2002 Image analysis for non-destructive and non-
702 invasive quantification of root growth and soil water content in
703 rhizotrons. Journal of Plant Nutrition and Soil Science 165: 573-581.

704 Kuijken RC, van Eeuwijk FA, Marcelis LF, Bouwmeester HJ 2015 Root
 705 phenotyping: from component trait in the lab to breeding. *Journal of*
 706 *Experimental Botany* 66: 5389-5401.

707 Kutschera L 1960 *Wurzelatlas mitteleuropäischer Ackerunkräuter und*
 708 *Kulturpflanzen*. DLG-Verlag, Frankfurt/Main.

709 Landl M, Huber K, Schnepf A, Vanderborght J, Javaux M, Bengough AG,
 710 Vereecken H 2017 A new model for root growth in soil with
 711 macropores. *Plant and Soil* 415: 99-116.

712 Le Bot J, Serra V, Fabre J, Draye X, Adamowicz S, Pagès L 2010 DART: a
 713 software to analyse root system architecture and development from
 714 captured images. *Plant and Soil* 326: 261-273.

715 Leitner D, Felderer B, Vontobel P, Schnepf A 2014 Recovering root system
 716 traits using image analysis exemplified by two-dimensional neutron
 717 radiography images of lupine. *Plant Physiology* 164: 24-35.

718 Leitner D, Klepsch S, Bodner G, Schnepf A 2010 A dynamic root system
 719 growth model based on L-Systems. *Plant and Soil* 332: 177-192.

720 Liang J, Zhang J, Wong M 1996 Effects of air-filled soil porosity and aeration
 721 on the initiation and growth of secondary roots of maize (*Zea mays*).
 722 *Plant and Soil* 186: 245-254.

723 Lichtenegger E, Kutschera L, Sobotik M 2009 *Wurzelatlas der Kulturpflanzen*
 724 *gemäßigter Gebiete: mit Arten des Feldgemüsebaues*. DLG-Verlag
 725 Frankfurt/Main.

726 Lynch JP 2007 Roots of the second green revolution. *Australian Journal of*
 727 *Botany* 55: 493-512.

728 Lynch JP, Nielsen KL, Davis RD, Jablókow AG 1997 SimRoot: modelling and
 729 visualization of root systems. *Plant and Soil* 188: 139-151.

730 Mairhofer S, Zappala S, Tracy SR, Sturrock C, Bennett M, Mooney SJ,
 731 Pridmore T 2012 RooTrak: automated recovery of three-dimensional

732 plant root architecture in soil from X-ray microcomputed tomography
 733 images using visual tracking. *Plant Physiology* 158: 561-569.

734 Mooney SJ, Pridmore TP, Helliwell J, Bennett MJ 2012 Developing X-ray
 735 computed tomography to non-invasively image 3-D root systems
 736 architecture in soil. *Plant and Soil* 352: 1-22.

737 Nagel K, Putz A, Gilmer F, Heinz K, Fischbach A, Pfeifer J, Faget M, Bloßfeld
 738 S, Ernst M, Dimaki C, Kastenholz B, Kleinert A, Galinski A, Scharr H,
 739 Fiorani F, Schurr U 2012 GROWSCREEN-Rhizo is a novel
 740 phenotyping robot enabling simultaneous measurements of root and
 741 shoot growth for plants grown in soil-filled rhizotrons. *Functional*
 742 *Plant Biology* 39: 891-904.

743 Nagel KA, Bonnett D, Furbank R, Walter A, Schurr U, Watt M 2015
 744 Simultaneous effects of leaf irradiance and soil moisture on growth and
 745 root system architecture of novel wheat genotypes: implications for
 746 phenotyping. *Journal of Experimental Botany* 66: 5441-5452.

747 Nakamoto T 1994 Plagiogravitropism of maize roots. *Plant and Soil* 165: 327-
 748 332.

749 Nye PH, Tinker PB 1977 Solute movement in the soil-root system. Univ of
 750 California Press.

751 Pagès L 2011 Links between root developmental traits and foraging
 752 performance. *Plant, Cell and Environment* 34: 1749-1760.

753 Pagès L, Pellerin S 1994 Evaluation of parameters describing the root system
 754 architecture of field grown maize plants (*Zea mays* L.), II. *Plant and*
 755 *Soil* 164: 169-176.

756 Pagès L, Picon-Cochard, Catherine 2014 Modelling the root system architecture
 757 of Poaceae. Can we simulate integrated traits from morphological
 758 parameters of growth and branching? *New Phytologist* 204: 149-158.

759 Pagès L, Vercambre G, Drouet J-L, Lecompte F, Collet C, Le Bot J 2004 Root
 760 Typ: a generic model to depict and analyse the root system architecture.
 761 Plant and Soil 258: 103-119.

762 Pellerin S, Pagès L 1994 Evaluation of parameters describing the root system
 763 architecture of field grown maize plants (*Zea mays* L.), I. Plant and Soil
 764 164: 155-167.

765 Pellerin S, Tabourel F 1995 Length of the apical unbranched zone of maize axile
 766 roots: its relationship to root elongation rate. Environmental and
 767 Experimental Botany 35: 193-200.

768 Pohlmeier A, Javaux M, Vereecken H, Haber-Pohlmeier S 2013 Magnetic
 769 resonance imaging techniques for visualization of root growth and root
 770 water uptake processes. Soil–Water–Root Processes: Advances in
 771 Tomography and Imaging: 137-156.

772 Popova L, van Dusschoten D, Nagel KA, Fiorani F, Mazzolai B 2016 Plant root
 773 tortuosity: an indicator of root path formation in soil with different
 774 composition and density. Annals of Botany 118: 685-698.

775 Postma JA, Dathe A, Lynch JP 2014 The optimal lateral root branching density
 776 for maize depends on nitrogen and phosphorus availability. Plant
 777 Physiology 166: 590-602.

778 Rascher U, Blossfeld S, Fiorani F, Jahnke S, Jansen M, Kuhn AJ, Matsubara S,
 779 Martin LL, Merchant A, Metzner R 2011 Non-invasive approaches for
 780 phenotyping of enhanced performance traits in bean. Functional Plant
 781 Biology 38: 968-983.

782 Rich S, Watt M 2013 Soil conditions and cereal root system architecture: review
 783 and considerations for linking Darwin and Weaver. Journal of
 784 Experimental Botany 64: 1193-1208.

785 Roose T, Schnepf A 2008 Mathematical models of plant–soil interaction.
 786 Philosophical Transactions of the Royal Society of London A:
 787 Mathematical, Physical and Engineering Sciences 366: 4597-4611.
 788 Schenk M, Barber S 1979 Phosphate uptake by corn as affected by soil
 789 characteristics and root morphology. Soil Science Society of America
 790 Journal 43: 880-883.
 791 Smith S, De Smet I 2012 Root system architecture: insights from Arabidopsis
 792 and cereal crops. Philosophical Transactions of the Royal Society B:
 793 Biological Sciences 367: 1441-1452.
 794 Tardieu F, Pellerin S 1990 Trajectory of the nodal roots of maize in fields with
 795 low mechanical constraints. Plant and Soil 124: 39-45.
 796 Tracy SR, Black CR, Roberts JA, Sturrock C, Mairhofer S, Craigon J, Mooney
 797 SJ 2012 Quantifying the impact of soil compaction on root system
 798 architecture in tomato (*Solanum lycopersicum*) by X-ray micro-
 799 computed tomography. Annals of Botany 110: 511-519.
 800 Tracy SR, Roberts JA, Black CR, McNeill A, Davidson R, Mooney SJ 2010 The
 801 X-factor: visualizing undisturbed root architecture in soils using X-ray
 802 computed tomography. Journal of Experimental Botany 61: 311-313.
 803 Tricot F, Crozat Y, Pellerin S 1997 Root system growth and nodule
 804 establishment on pea (*Pisum sativum* L.). Journal of Experimental
 805 Botany 48: 1935-1941.
 806 Volder A, Smart DR, Bloom AJ, Eissenstat DM 2005 Rapid decline in nitrate
 807 uptake and respiration with age in fine lateral roots of grape:
 808 implications for root efficiency and competitive effectiveness. New
 809 Phytologist 165: 493-502.
 810 Weaver JE, Jean FC, Crist JW 1922 Development and activities of roots of crop
 811 plants: a study in crop ecology. Carnegie Institution of Washington,
 812 United States.

813 Weaver JE, Kramer J, Reed M 1924 Development of Root and Shoot of Winter
814 Wheat Under Field Environment. *Ecology* 5: 26-50.

815 Wenzel WW, Wieshammer G, Fitz WJ, Puschenreiter M 2001 Novel rhizobox
816 design to assess rhizosphere characteristics at high spatial resolution.
817 *Plant and Soil* 237: 37-45.

818 Wu J, Pagès L, Wu Q, Yang B, Guo Y 2015 Three-dimensional architecture of
819 axile roots of field-grown maize. *Plant and Soil* 387: 363-377.

820 Wu L, McGechan M, McRoberts N, Baddeley J, Watson C 2007 SPACSYS:
821 integration of a 3D root architecture component to carbon, nitrogen and
822 water cycling—model description. *Ecological Modelling* 200: 343-359.

823 Wu L, McGechan M, Watson C, Baddeley J 2005 Developing existing plant
824 root system architecture models to meet future agricultural challenges.
825 *Advances in Agronomy* 85: 181-219.

826 Yu P, Gutjahr C, Li C, Hochholdinger F 2016 Genetic control of lateral root
827 formation in cereals. *Trends in Plant Science* 21: 951-961.

Table 1: Overview of the parametrization of the root traits inter-branch distance, branching angle and directional orientation of root segments in the different 3D root architecture models; L...length unit, T... time unit

	RootTyp (Pagès et al. 2004)	SimRoot (Lynch et al. 1997)	ROOTMAP (Diggle 1988)	SPACSYS (Wu et al. 2007)	R-SWMS (Javaux et al. 2008)	RootBox (Leitner et al. 2010)
Inter-branch distance	Fixed value or increasing values with depth (L) specified for each root order	Fixed value (L) specified for each root order	Fixed value (L) specified for each root order	Fixed value (L) specified for each root order	Fixed value (T) specified for each root order (inter-branch distance is then also a function of root growth rate)	Drawn from truncated normal distribution (L) with mean and standard deviation specified for each order
Branching angle	Drawn from normal distribution with mean and standard deviation specified for each root order	Fixed value specified for each root order	Fixed at 90° to its parent root	Initial value with random variation within a predefined range	Fixed value specified for each root order	Drawn from normal distribution with mean and standard deviation specified for each order
Directional orientation of root segments	Computed from the direction of the previous root segment, different selectable tropisms and a random deflection angle	Computed from the direction of the previous root segment, gravitropism and a random deflection angle	Stochastically determined with the help of a random deflection angle that is calculated on the basis of a user defined probability and a gravitropism index	Computed from the direction of the previous root segment, gravitropism and a random deflection angle, which is scaled with the maximum root segment length	Computed from the direction of the previous root segment, plagiogravitropism and a random deflection angle, which is scaled with the maximum root segment length	A random angle, which is scaled with the root segment length, is added to the growth direction of the previous root segment; this random angle is selected for its directional proximity to a desired selectable tropism from a specified number of random angle realizations

Table 2: Description of image sources from literature; SW...spring wheat, WW...winter wheat

Image Number	Variety	Root system age (calendar days)	Location	Literature source
1	SW	60	Peru, Nebraska, US	Weaver et al. (1922)
2	SW	70		
3	SW	93		
4	SW	93		
5	WW	20	Lincoln, Nebraska, US	Weaver et al. (1922), Weaver et al. (1924)
6	WW	30		
7	SW	31		
8	SW	45		
9	SW	60		
10	WW	60	St. Donat,	Lichtenegger et al. (2009)
11	WW	60	Carinthia, Austria	

Table 3: Parameter values for simulation; sg... sensitivity to gravitropism (-), σ ... unit standard deviation of the random angle ($^{\circ}\text{cm}^{-1}$), parameter explanations can be found in Clausnitzer and Hopmans (1994)

Gravitropism component	Tortuosity component
sg = [0.005; 0.01; 0.05; 0.1; 0.15; 0.2; 0.25; 0.3; 0.35; 0.4]	
$\sigma = 0$ to 20, interval = 1	

Table 4: Variation intervals of focus parameters; parameter explanations are found in Leitner et al. (2010)

Parameter	Factor	Unit	Root order	min	max
Inter-branch distance	μ	(cm)	Axial	0.1	0.5
	std	(cm)	Axial	0	0.5
Branching angle	μ	($^{\circ}$)	1 st order lateral	60	90
	std	($^{\circ}$)	1 st order lateral	0	50
Root growth trajectories	std of random angle	($^{\circ}\text{cm}^{-1}$)	Axial	9	20
	deflection / tortuosity				
	Sensitivity to gravitropism	(-)	Axial	0.01	0.3
Additional factors:		Normally / lognormally distributed inter-branch distance Random / regular radial branching angle			

Table 5: Constant parameter values; parameter explanations are found in Leitner et al. (2010)

Parameter	Unit	axis	1 st order laterals	2 nd order laterals
Initial elongation rate	(cm d^{-1})	1.2 ^a	0.8 ^a	0.8 ^a
Root radius	(cm)	0.038 ^a	0.027 ^a	0.027 ^a
Basal root zone	(cm)	2	0.2 ^c	0.125
Apical root zone	(cm)	6	0.3 ^c	0.125
Inter-branch distance	(cm)	fp	0.25	0
Number of branches per root axis	(-)	50	6 ^c	0
Insertion/Branching angle	($^{\circ}$)	70	fp	90
Tropism	(-)	Gravitropism	Exotropism	Exotropism
Tropism sensitivity	sg (-)	fp	0.1	0.1
std of random angle deflection	σ ($^{\circ}\text{cm}^{-1}$)	fp	20	20

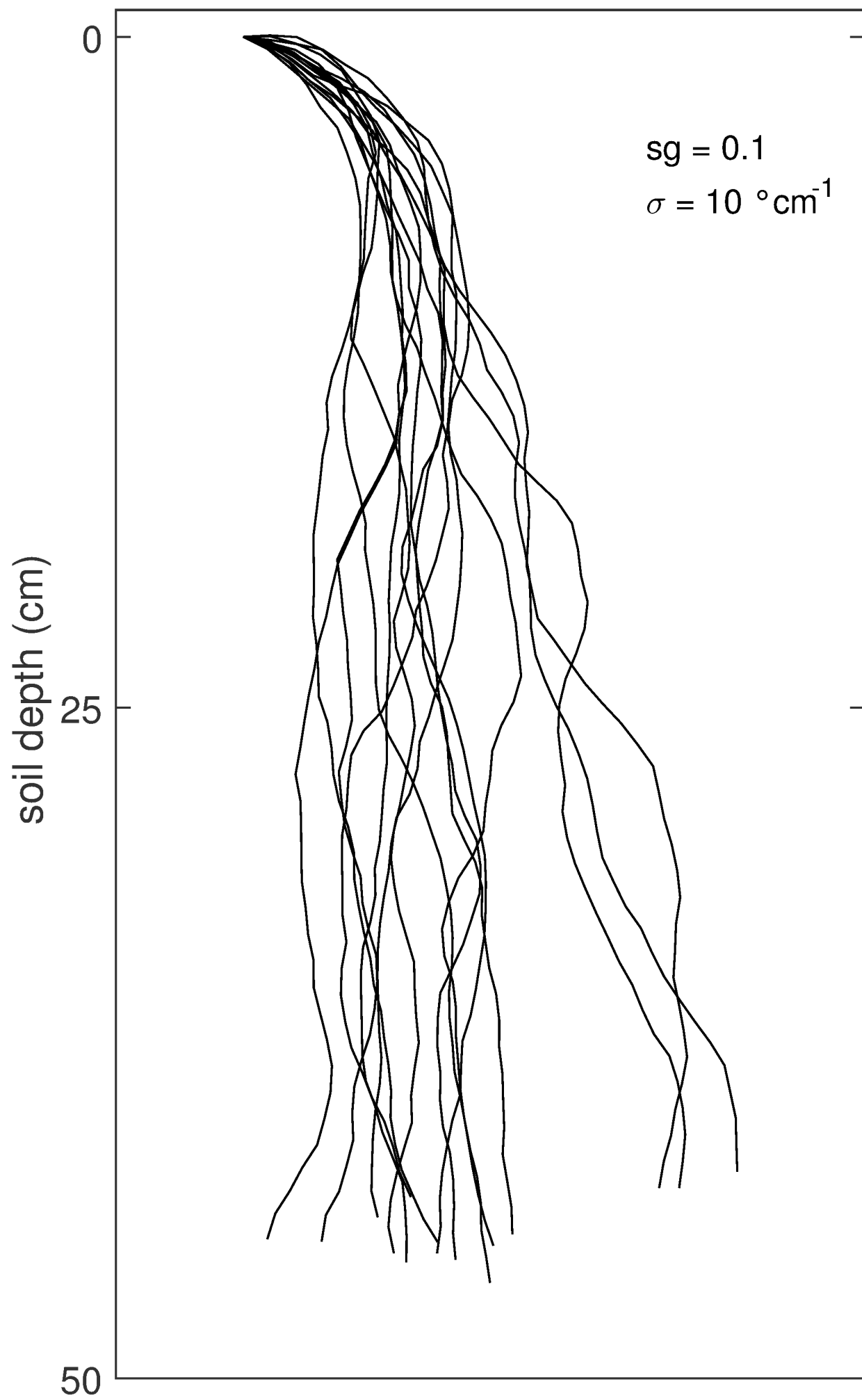
fp... focus parameter, specified in Table 4

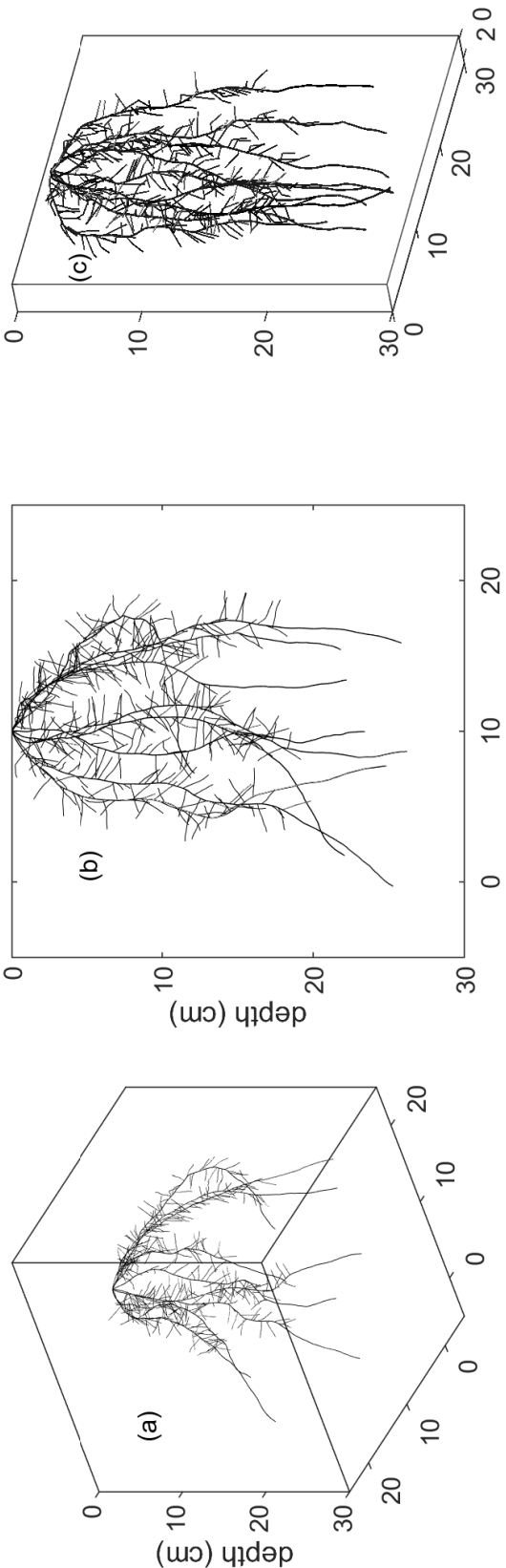
^a based on Materechera et al. (1991)^b based on Ito et al. (2006)^c derived from root lengths of 1st order laterals given by Ito et al. (2006)Table 6: Correlation coefficients between inter-root competition and parametrization factors, bold characters represent significant values at $p < 0.05$

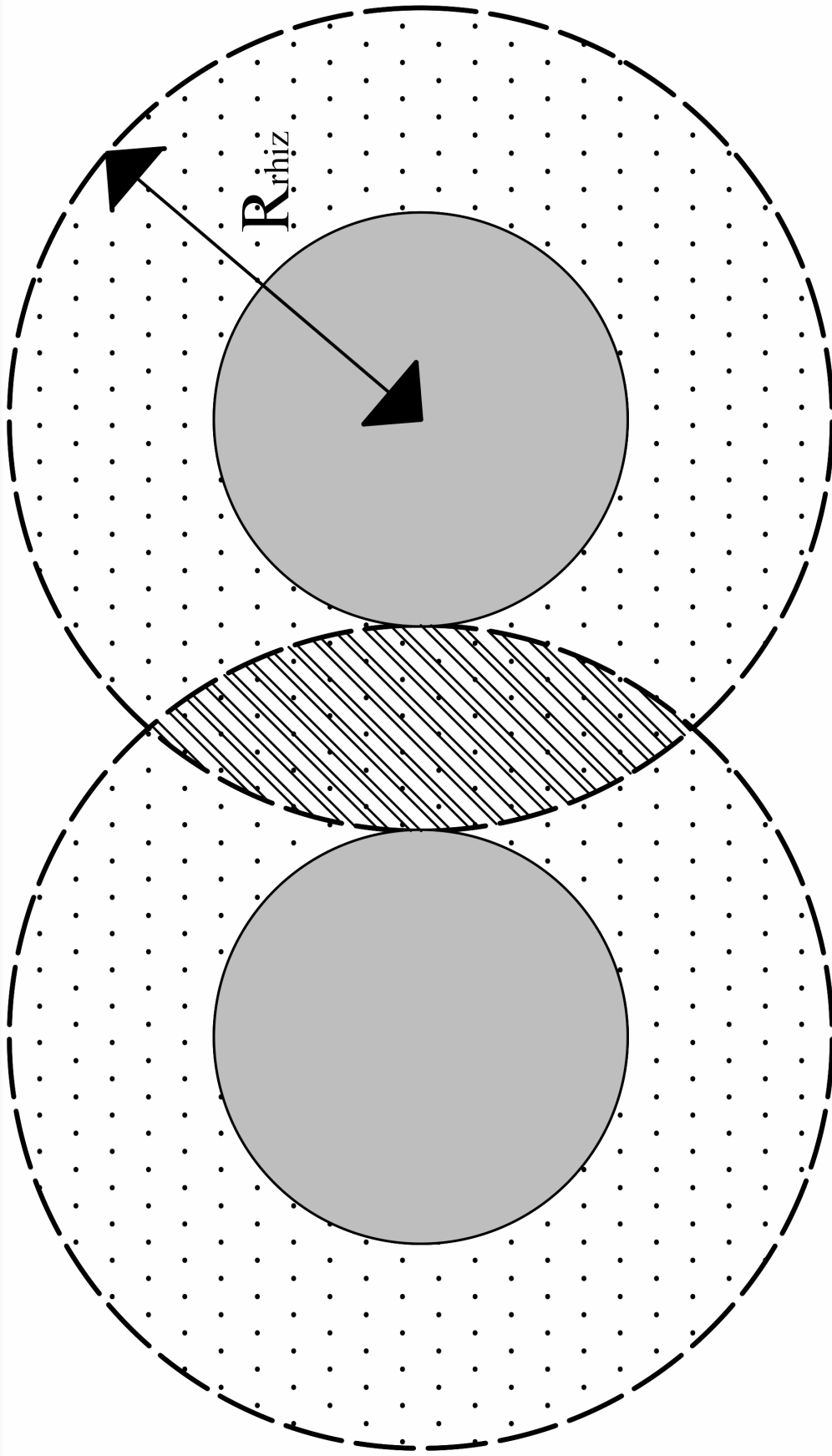
	ibd, μ	ibd, std	θ , μ	θ , std	σ	sg
--	------------	----------	------------------	----------------	----------	----

$D_e = 10^{-8} \text{ cm}^2\text{s}^{-1}$	norm, rand	-0.78	-0.20	-0.08	0.30	-0.07	0.32
	norm, reg	-0.76	-0.12	-0.07	0.36	-0.05	0.32
	lognorm, rand	-0.81	0.17	-0.09	0.18	-0.06	0.26
	lognorm, reg	-0.83	0.08	-0.07	0.25	-0.06	0.22
$D_e = 10^{-7} \text{ cm}^2\text{s}^{-1}$	norm, rand	-0.81	-0.25	-0.02	0.16	-0.07	0.32
	norm, reg	-0.80	-0.17	0.01	0.20	-0.06	0.32
	lognorm, rand	-0.82	0.12	-0.03	0.09	-0.05	0.27
	lognorm, reg	-0.85	0.03	0.00	0.13	-0.08	0.24
$D_e = 2 \times 10^{-6} \text{ cm}^2\text{s}^{-1}$	norm, rand	-0.73	-0.24	0.00	0.04	-0.09	0.49
	norm, reg	-0.72	-0.17	0.06	0.04	-0.10	0.49
	lognorm, rand	-0.70	0.04	0.01	0.01	-0.07	0.45
	lognorm, reg	-0.72	-0.06	0.02	0.01	-0.12	0.43

norm / lognorm... normally / lognormally distributed inter-branch distances, rand / reg... random / regular alignment
of 1st order laterals around the root axis



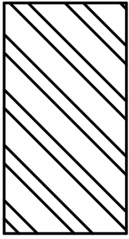
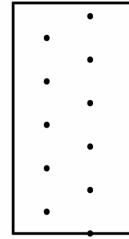


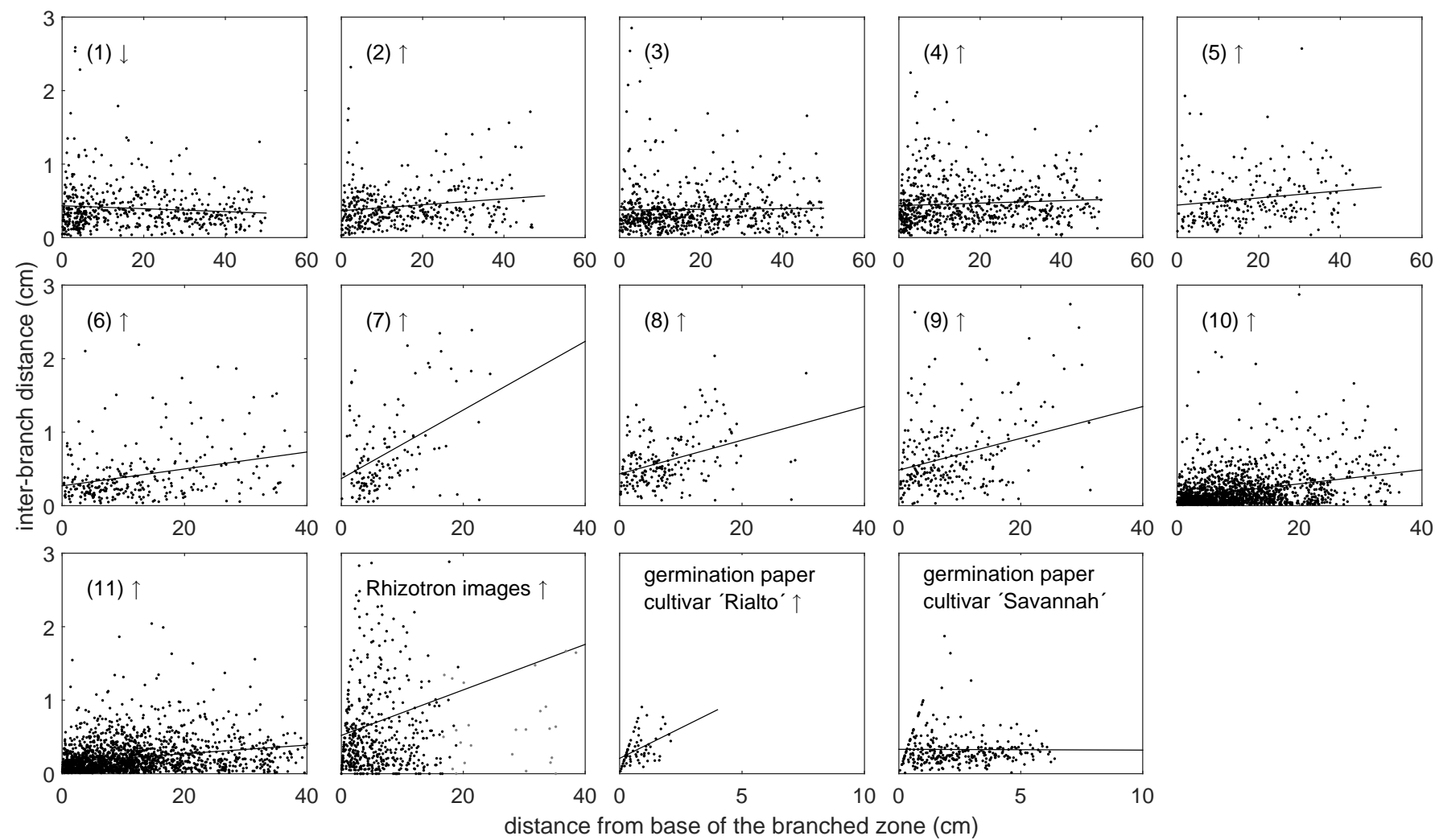


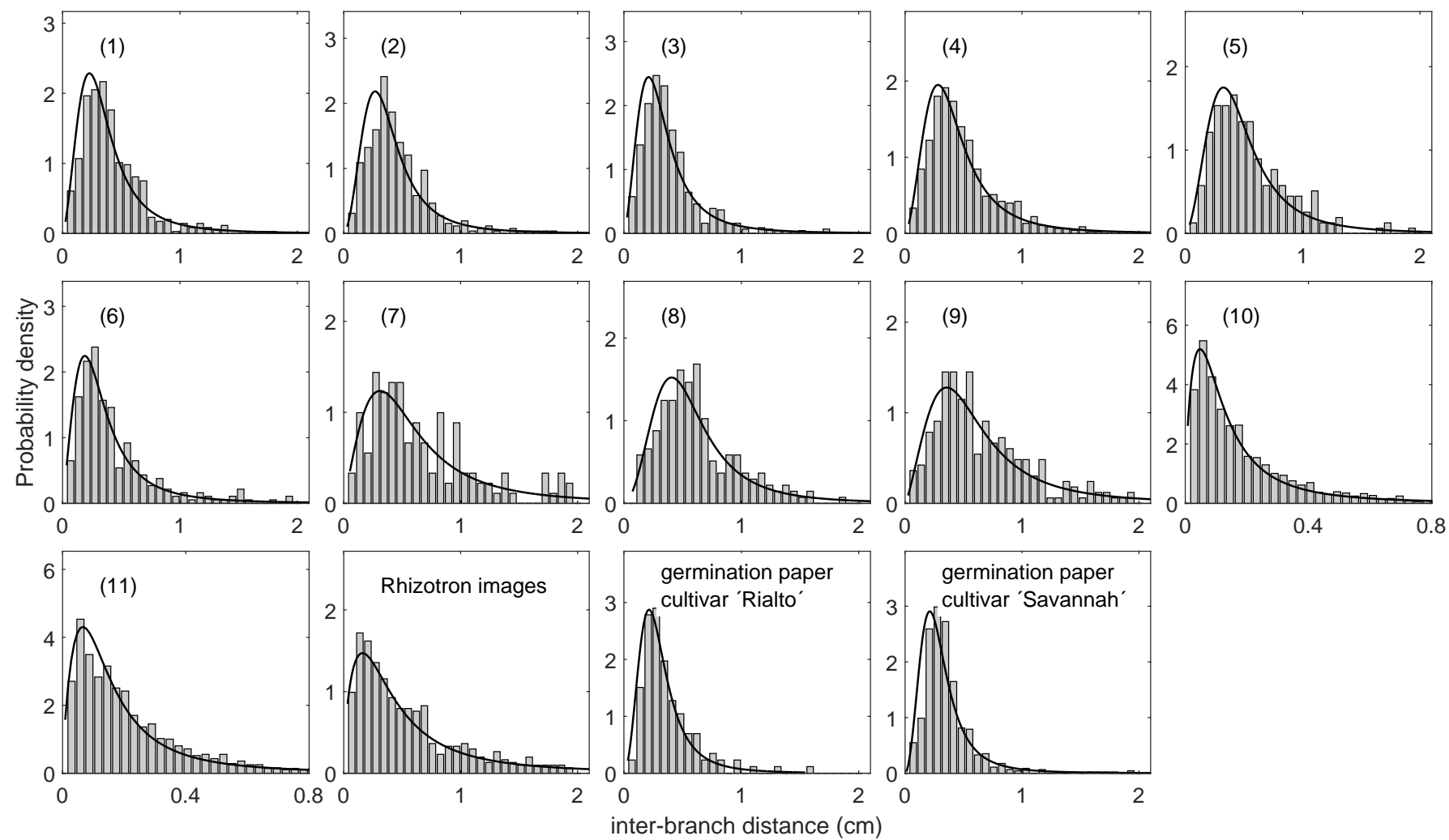
cross-section through roots

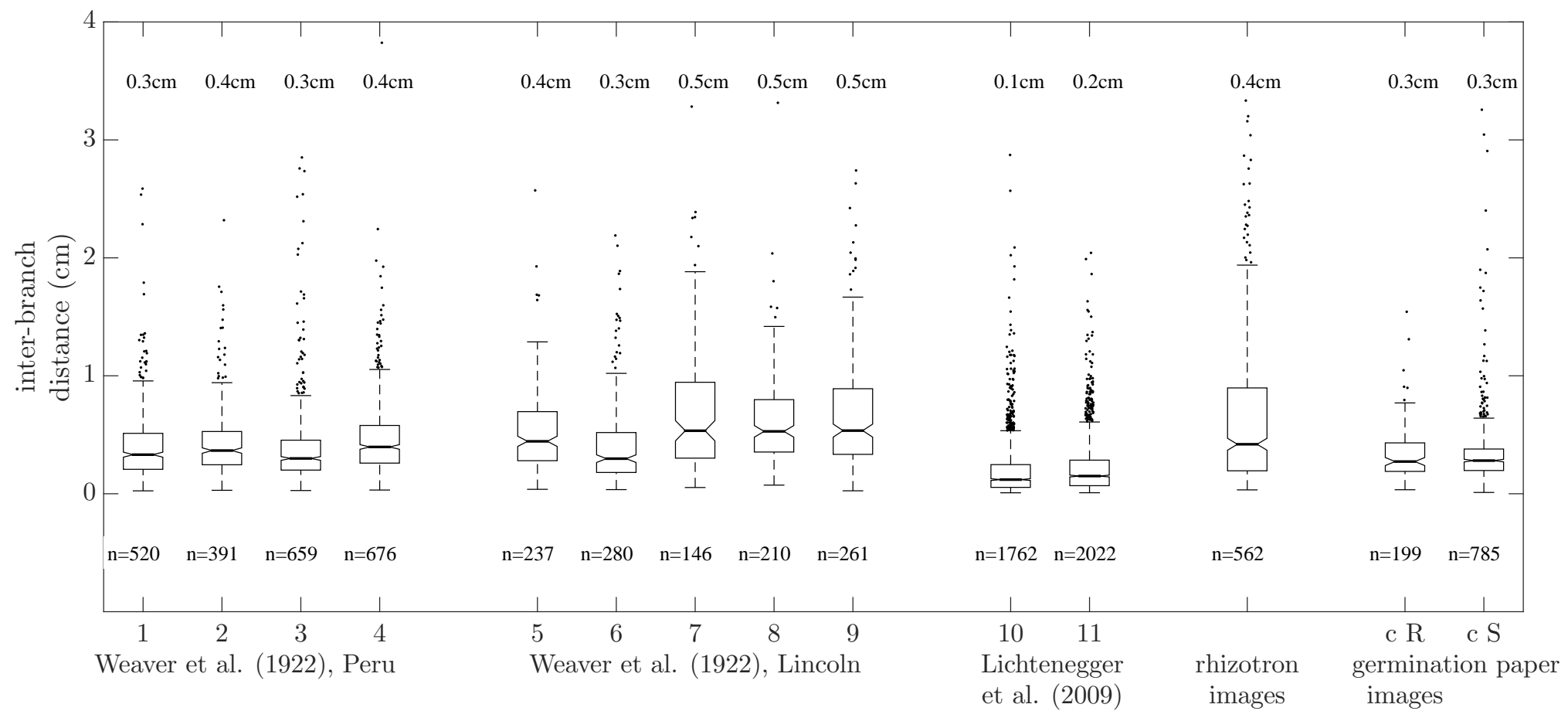
net rhizosphere volume

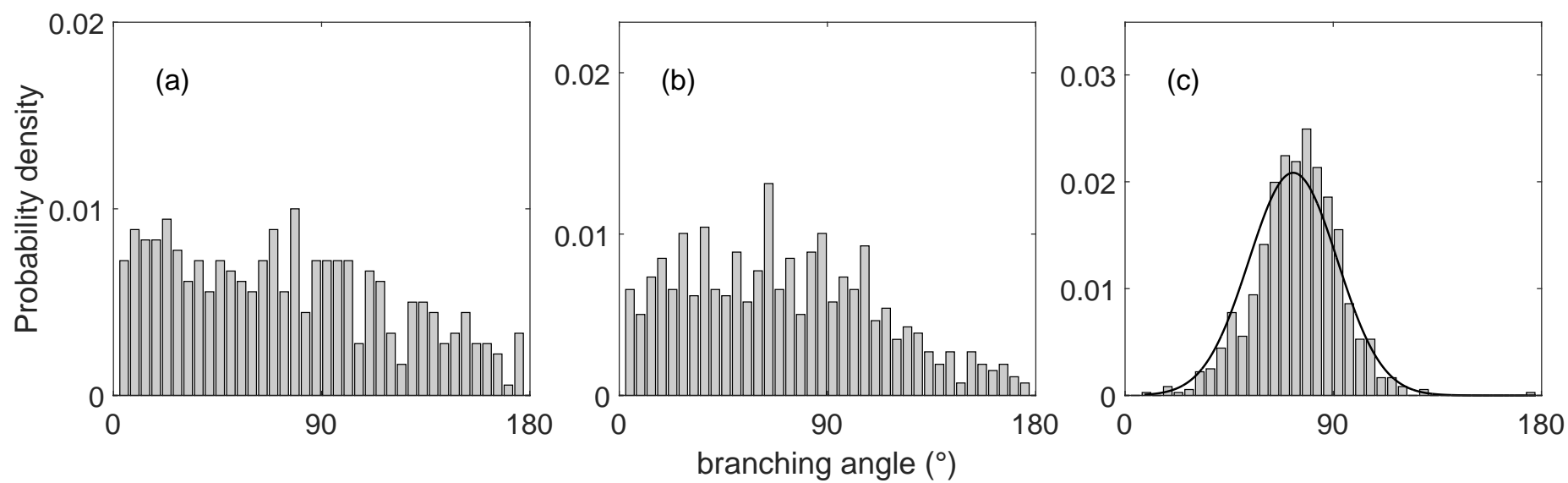
overlap volume

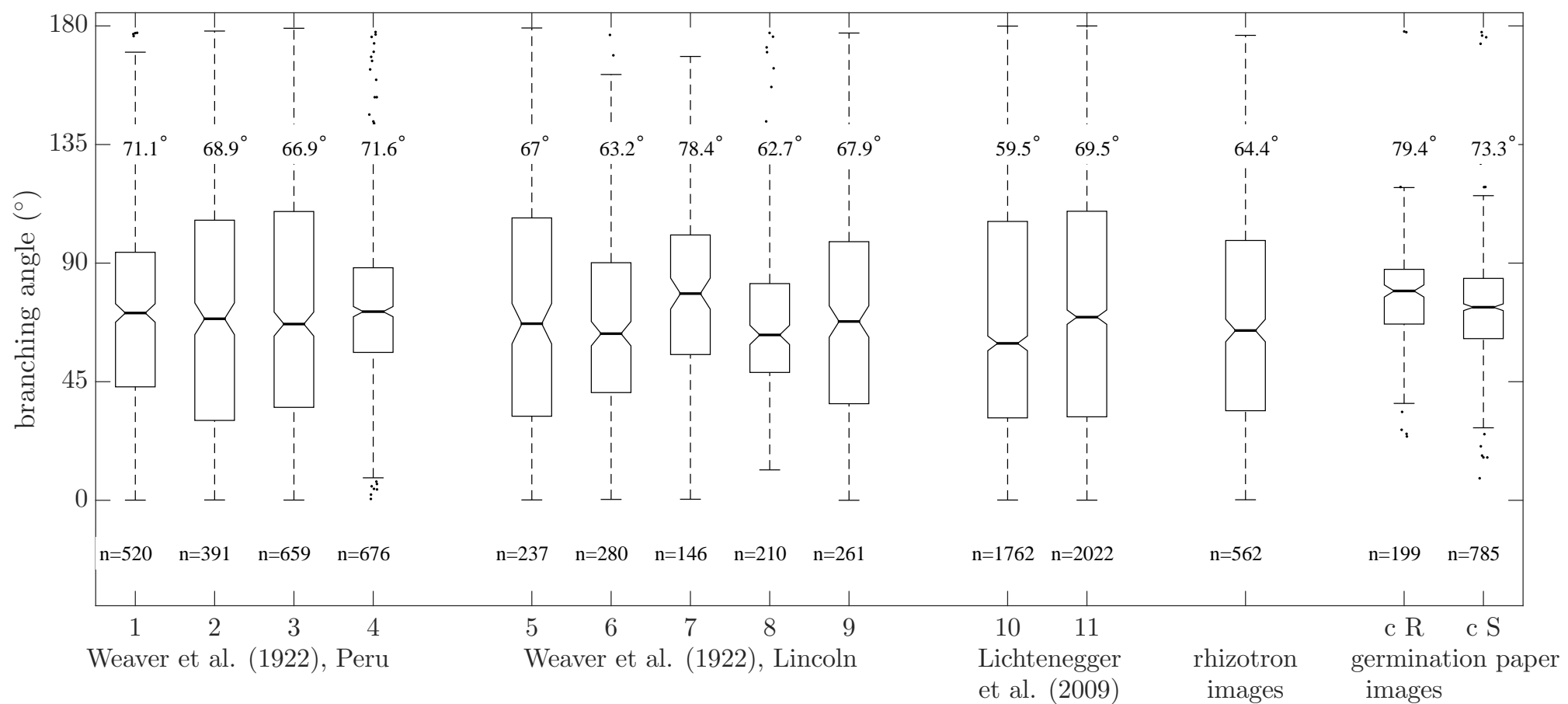


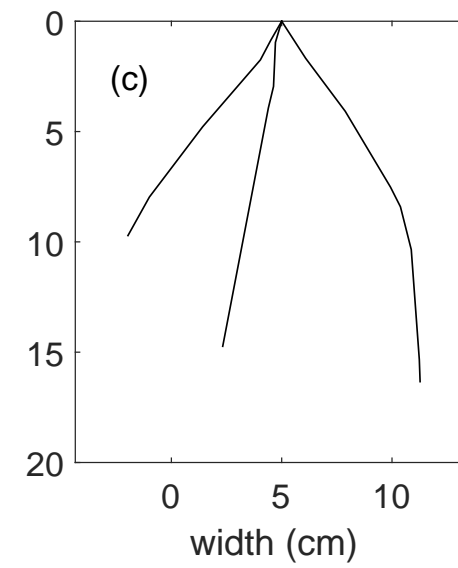
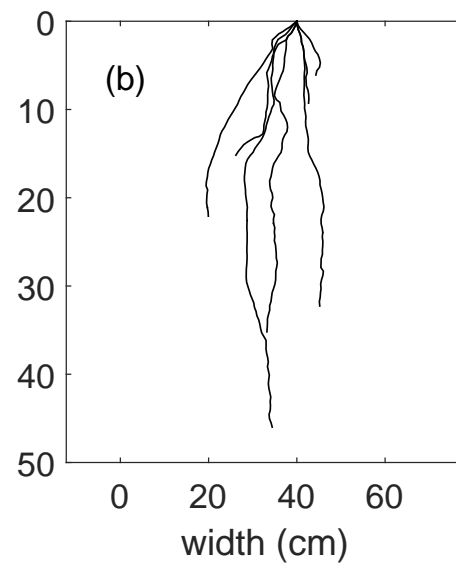
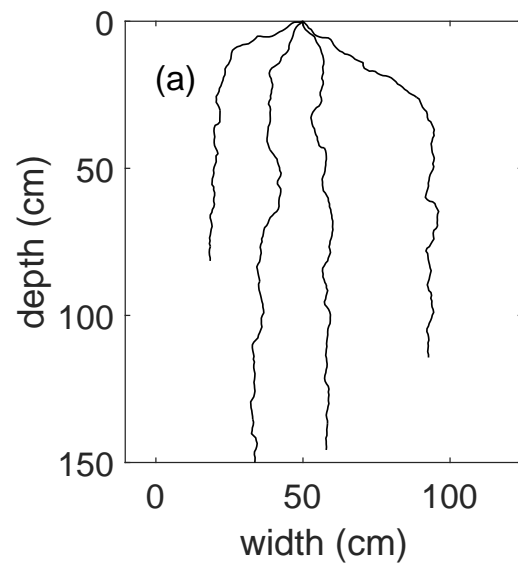


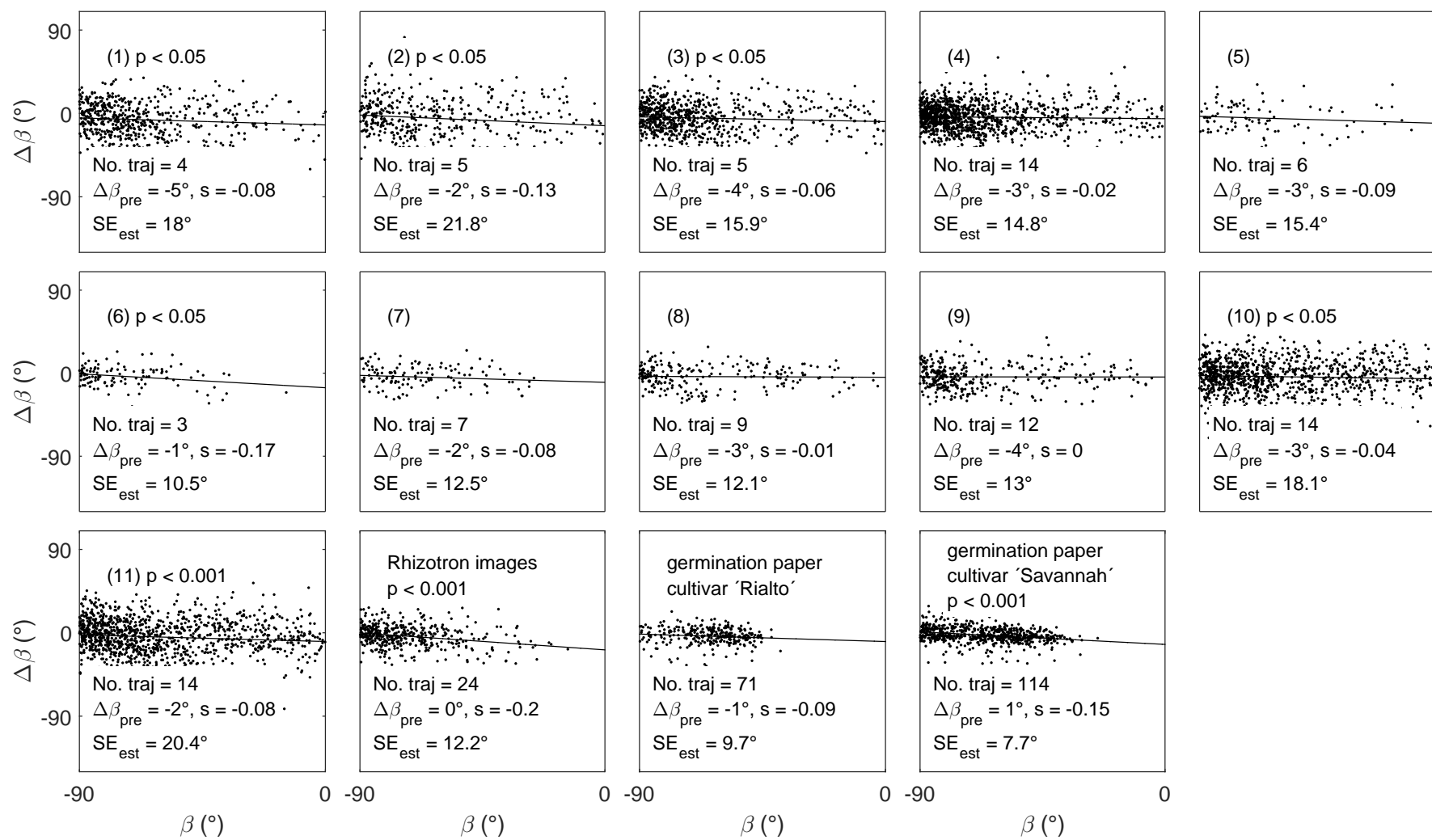


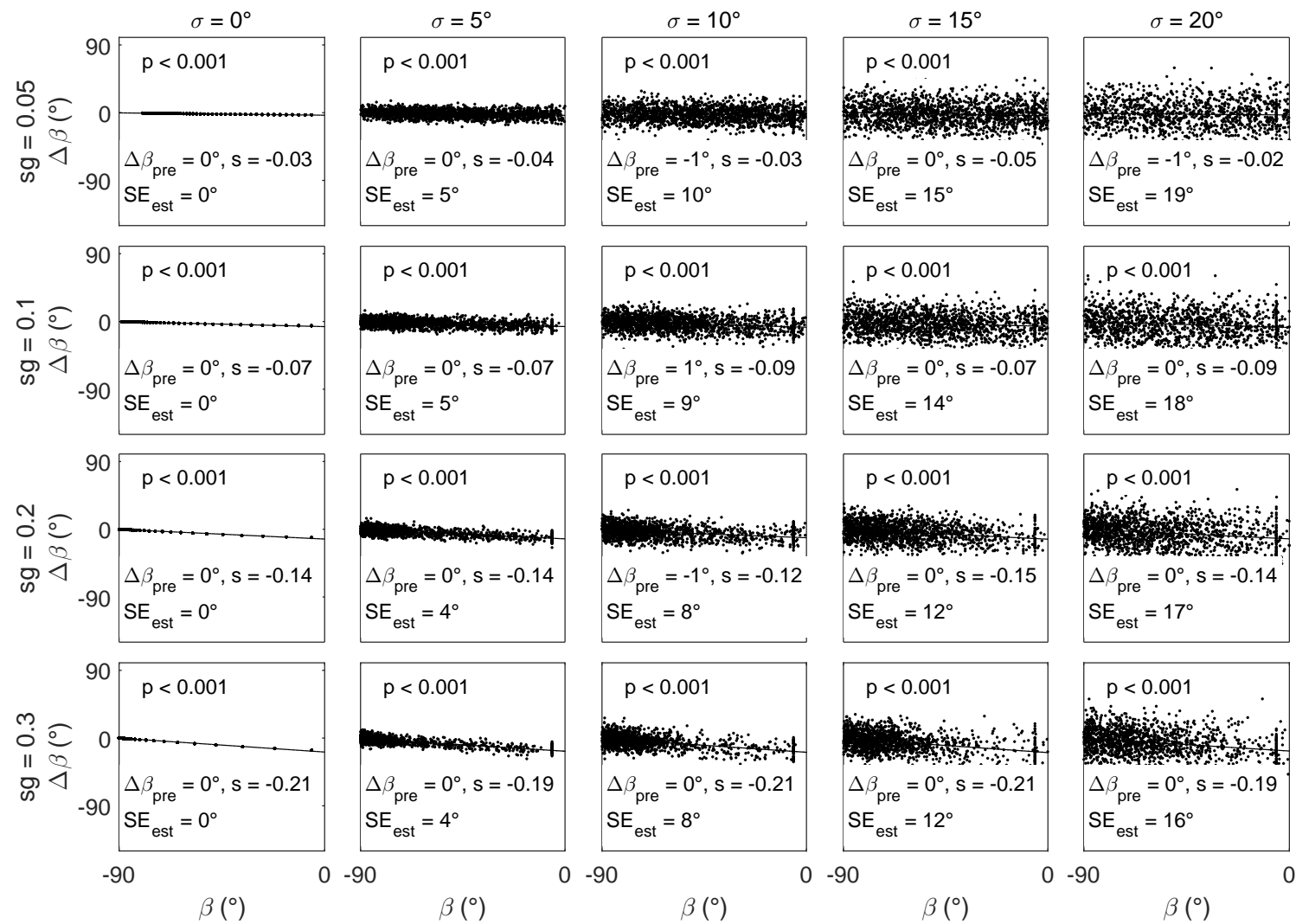


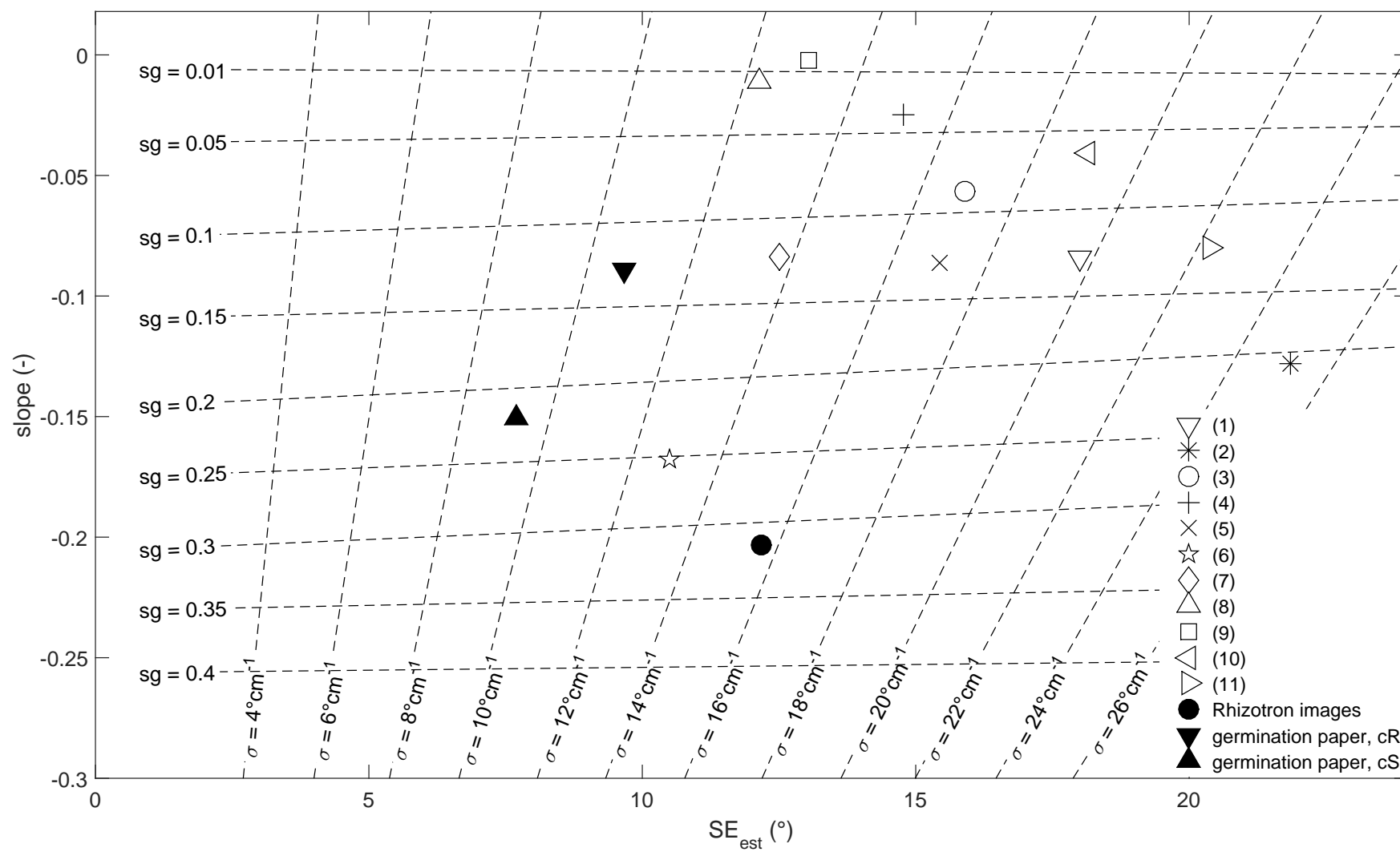


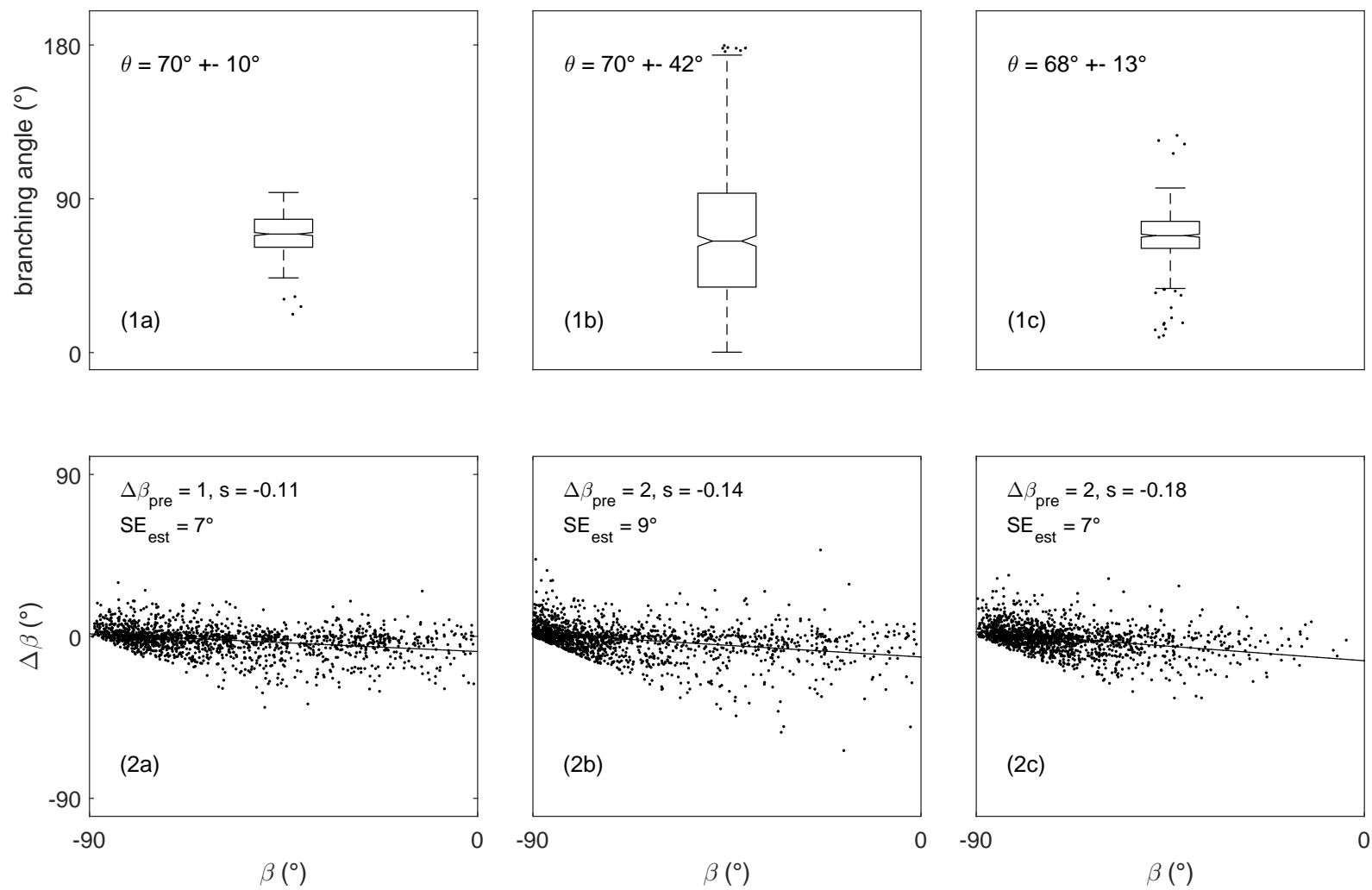


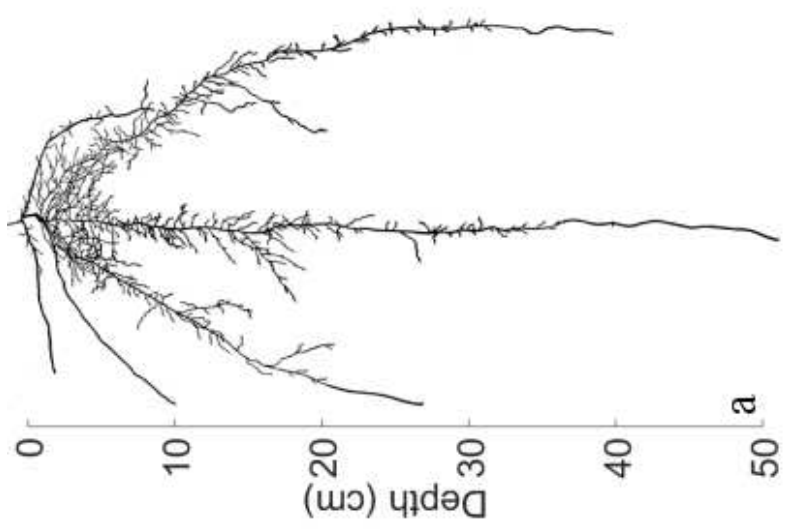
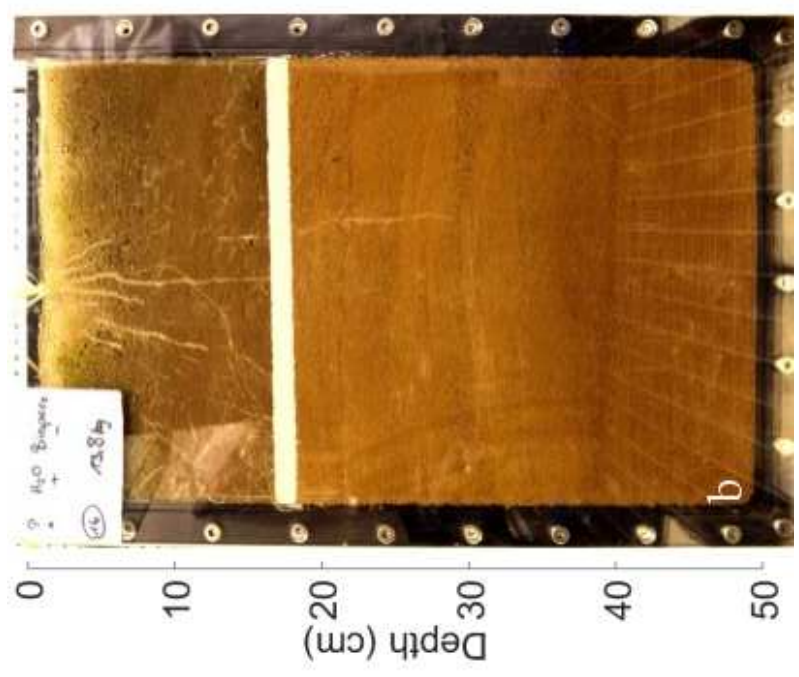
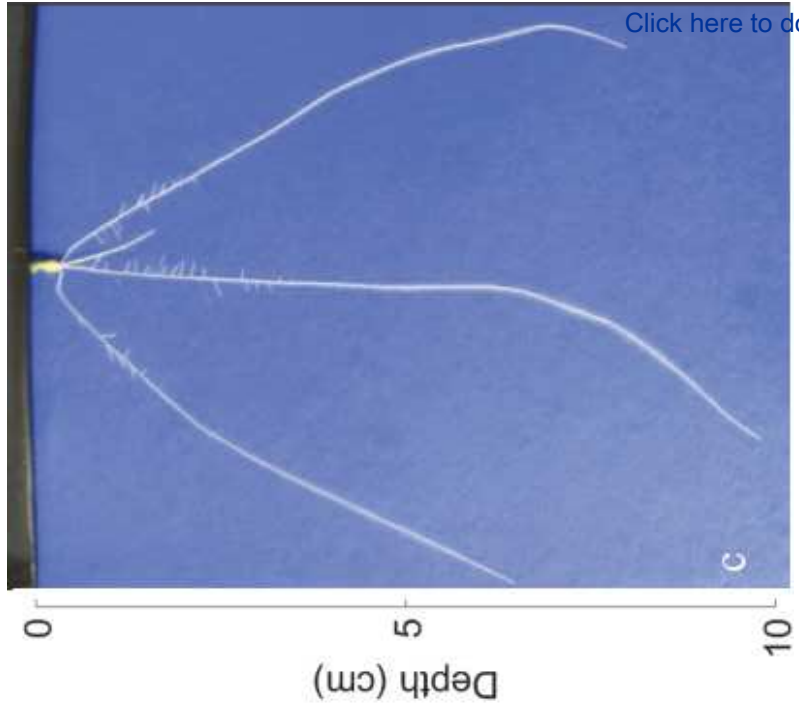


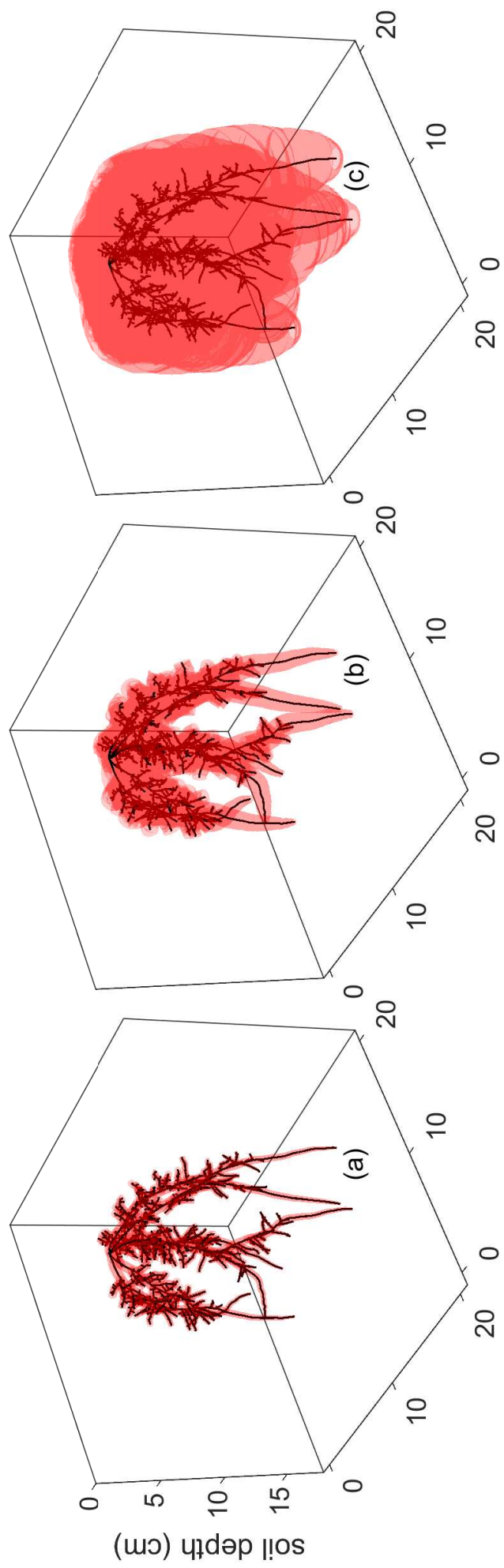












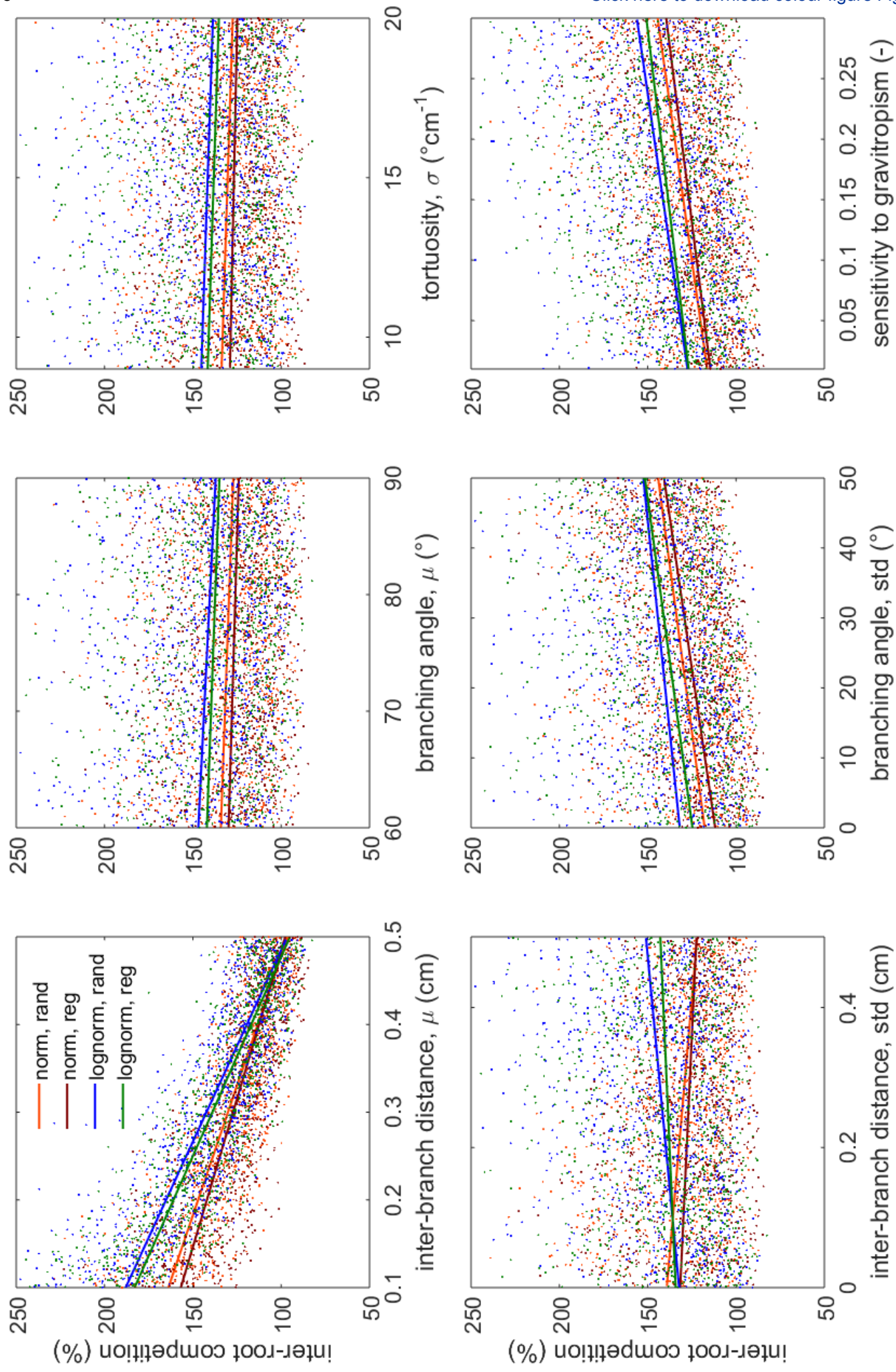


Fig. 1 Example images for each data source: (a) root drawing, (b) rhizotron image, (c) image of roots grown on germination paper

Fig. 2 Example of simulated axial root trajectories

Fig. 3 ROOTBOX simulations of (a) unconstrained root growth in 3D, (b) unconstrained root growth projected onto xz- plane, (c) constrained root growth in a rhizotron

Fig. 4 Schematic representation of rhizosphere volume, overlap volume and rhizosphere radius R_{rhiz} : grey circles represent cross-sections through two individual roots, dotted and diagonal hatching show net rhizosphere and overlap volume, respectively

Fig. 5 Representation of the computed 3D root system (black) with rhizosphere zone (red) for simulations with $D_e = 10^{-8} \text{ cm}^2\text{s}^{-1}$ (a), $D_e = 10^{-7} \text{ cm}^2\text{s}^{-1}$ (b) and $D_e = 2 \times 10^{-6} \text{ cm}^2\text{s}^{-1}$ (c) at day 30

Fig. 6 Relationship between inter-branch distance and distance from the base of the branched zone illustrated for each data source; arrows indicate a significant up- respectively downward trend in the data set; the number codes for data sources one to eleven are found in Table 2

Fig. 7 Probability distributions of inter-branch distances with fitted lognormal functions illustrated for each data source; data sets were plotted using different scales for x- and y-axis; the number codes for data sources one to eleven are found in Table 2

Fig. 8 Variation of inter-branch distances, medians, quartile ranges and sample sizes (n) for the different data sources; the number codes for data sources one to eleven are found in Table 2; cR...cultivar Rialto, cS... cultivar Savannah

Fig. 9 Examples of probability distributions of branching angles for (a) a root drawing, (b) a rhizotron image, (c) an image of roots grown on germination paper with fitted normal function

Fig. 10 Variation of branching angles, medians, quartile ranges and sample sizes (n) for the different data sources; the number codes for data sources one to eleven are found in Table 2; cR...cultivar Rialto, cS... cultivar Savannah

Fig. 11 Examples of reconstructed root growth trajectories of the axial roots for (a) a root drawing, (b) a rhizotron image, (c) an image of roots grown on germination paper

Fig. 12 Relationship between reorientation angle $\Delta\beta$ and angle of the previous 1cm long axial root section β for each data source; $\Delta\beta_{pre}...$ $\Delta\beta$ predicted by regression at $\beta=-90^\circ$; s...slope, SEest... standard error of the estimate; No. traj ... number of analyzed trajectories; the number codes for data sources one to eleven are found in Table 2

Fig. 13 Relationship between reorientation angle $\Delta\beta$ and angle of the previous 1cm long axial root section β for simulated root systems using different parameterizations of the sensitivity to gravitropism sg and the unit standard deviation of the random angle σ ; $\Delta\beta_{pre}...$ $\Delta\beta$ predicted by regression at $\beta=-90^\circ$, s...slope, SEest... standard error of the estimate. $\beta=-90^\circ$ corresponds to a root segment growing vertically downwards, $\beta=0^\circ$ to a horizontally growing root segment.

Fig. 14 Characteristic curves for the deduction of the gravitropism parameter sg and the tortuosity parameter σ from the properties of the regression line (standard error of the estimate SEest and slope) that relates root reorientation and root angle. The value pair of regression line properties of each data source deduced from Fig.12 is inserted into the graph; the number codes for data sources one to eleven are found in Table 2

Fig. 15 (1) Branching angle θ (mean +- standard deviation) and (2) relationship between reorientation angle $\Delta\beta$ and angle of the previous 1 cm long axile root section β with $\Delta\beta_{pre}...$ $\Delta\beta$ predicted by regression at $\beta=-90^\circ$, s...slope, SEest... standard error of the estimate for (a) unconstrained root growth in 3D, (b) unconstrained root growth projected onto the xz- plane and (c) constrained root growth in a rhizotron (Fig.3)

Fig. 16 Scatter plots with linear regression lines illustrating the relationships between inter-root competition and different parameterization factors for $D_e = 10^{-8} \text{ cm}^2\text{s}^{-1}$; $\mu...$ mean value, std... standard deviation, norm / lognorm... normally / lognormally distributed inter-branch distances, rand / reg... random / regular alignment of 1st order laterals around the root axis